Tropical drought patterns and their linkages to large-scale climate variability over Peninsular Malaysia

He, Q., Chun, K. P., Tan, M. L., Dieppois, B., Liew, J., Klaus, J., Fournier, M., Massei, N. & Yetemen, O.

Original citation & hyperlink:
He, Q, Chun, KP, Tan, ML, Dieppois, B, Liew, J, Klaus, J, Fournier, M, Massei, N & Yetemen, O 2021, 'Tropical drought patterns and their linkages to large-scale climate variability over Peninsular Malaysia', Hydrological Processes, vol. 35, no. 9, e14356, pp. (In-Press).
https://dx.doi.org/10.1002/hyp.14356

DOI 10.1002/hyp.14356
ISSN 0885-6087
ESSN 1099-1085

Publisher: Wiley

Tropical drought patterns and their linkages to large-scale climate variability over Peninsular Malaysia

Running head: tropical drought linked to large-scale climate variability

Qing He[1], Kwok Pan Chun[1*], Mou Leong Tan[2], Bastien Dieppois[3, 4], Juneng Liew[5], Julian Klaus[6], Matthieu Fournier[7], Nicolas Massei[7], Omer Yetemen[8]

[1] Department of Geography, Hong Kong Baptist University, Hong Kong, China

[2] Geoinformatic Unit, Geography section, School of Humanities, Universiti Sains Malaysia, 11800 USM, Penang, Malaysia

[3] Centre for Agroecology, Water and Resilience, Coventry University, UK

[4] Department of Oceanography, University of Cape Town, South Africa

[5] Department of Earth Sciences and Environment, Faculty of Science and Technology, Universiti Kebangsaan Malaysia, Bangi, Malaysia

[6] Catchment and Eco-hydrology Research Group, Department of Environmental Research and Innovation, Luxembourg Institute of Science and Technology, Esch/Alzette, Luxembourg

[7] M2C Laboratory, The University of Rouen Normandy, France

[8] Eurasia Institute of Earth Sciences, Istanbul Technical University, Istanbul, Turkey

* Corresponding author:

Dr Kwok Pan Chun, kpchun@hkbu.edu.hk; Department of Geography, Hong Kong Baptist University, Hong Kong, China.

Abstract

Ocean-atmosphere modes of climate variability in the Pacific and Indian oceans, as well as monsoons, regulate the regional wet and dry episodes in tropical regions. However, how those modes of climate variability, and their interactions, lead to spatial differences in drought patterns over tropical Asia at seasonal- to interannual time scales remains unclear. This study aims to analyse the hydroclimate processes for both short- and long-term spatial drought patterns (3-, 6, 12- and 24-months) over Peninsular Malaysia using the Standardized Precipitation Index, Standardized Precipitation Evapotranspiration Index, and Palmer Drought Severity Index. Besides that, a generalised least squares regression is used to explore underlying circulation mechanisms of these spatio-temporal drought patterns. The tested drought indices indicate a tendency toward wetter conditions over Peninsular Malaysia. Based on principal component analysis, distinct spatio-temporal drought patterns are revealed, suggesting North-South and East-West gradients in drought distribution. The Pacific El Nino Southern Oscillation (ENSO), the South Western Indian Ocean (SWIO) variability, and the quasi-biennial oscillation (QBO) are significant contributors to the observed spatio-temporal variability in drought. Both the ENSO and the SWIO modulate the North-South gradient in drought conditions over Peninsular Malaysia, while the QBO contributes more to the East-West gradient. Through modulating regional moisture fluxes, the warm phases of the ENSO and the SWIO, and the western phases of the QBO weaken the southwest and northeast monsoon, leading to precipitation deficits and droughts over Peninsular Malaysia. The East-

West or North-South gradients in droughts are related to the middle mountains blocking southwest and northeast moisture fluxes toward Peninsular Malaysia. In addition, the ENSO and QBO variations are significantly leading to short-term droughts (less than a year), while the SWIO is significantly associated with longer-duration droughts (two years or more). Overall, this work demonstrates how spatio-temporal drought patterns in tropical regions are related to monsoons and moisture transports affected by the oscillations over the Pacific and Indian oceans, which is important for national water risk management.

Keywords: Peninsular Malaysia; Spatiotemporal droughts; El Nino Southern Oscillation (ENSO); South Western Indian Ocean (SWIO); Quasi-Biennial Oscillation (QBO); Tropical interannual variation

1. Introduction

Drought is one of the most disruptive natural hazards with recurrent features, which occurs in all climate zones (Liu et al., 2013; Sanusi, Jemain, Zin, & Zahari, 2015). Even though Peninsular Malaysia receives an average of around 2500 mm of precipitation per year, the region is affected by frequent episodes of drought in response to changes in climate (Chinnasamy & Ganapathy, 2017). The dry spells result in strong impacts on agricultural and socio-economic sectors, notably by reducing local paddy and oil palm production, which are the most important crops in Malaysia (Firdaus, Leong Tan, Rahmat, & Senevi Gunaratne, 2020; Nurul Fatin, Mohd Razali, Ahmad, & Mohd Shafri, 2019), and by enhancing the occurrence of forest wildfires and reducing the social stability over Peninsular Malaysia (Hui-Mean, Yusof, Yusop, & Suhaila, 2019; Yusof, Hui-Mean, Suhaila, & Yusof, 2013). While the social and ecological disturbances caused by short-term droughts (i.e. lasting less than a year) are generally manageable and recoverable, long-term droughts (i.e. lasting more than a year) can lead to irreversible hydrological and ecological changes (Munson, Bradford, & Hultine, 2020; Tallaksen & Van Lanen, 2004). Therefore, analysing droughts at different time scales,

especially long-term droughts, provides insights into regional water management and mitigation measures (Sun, Zhu, Pan, Zhang, & Liu, 2018).

Droughts are quantified and investigated through hydroclimate observations, including precipitation (McKee, Doesken, & Kleist, 1993; Valipour, 2016), evapotranspiration (ET; Chen & Sun, 2015; Vicente-Serrano, Beguería, & López-Moreno, 2010), streamflow (Shukla & Wood, 2008; Wu, Miao, Tang, Duan, & He, 2018), groundwater (Li & Rodell, 2015; Thomas et al., 2017), and soil moisture (Martínez-Fernández, González-Zamora, Sánchez, Gumuzzio, & Herrero-Jiménez, 2016; Wang, Lettenmaier, & Sheffield, 2011). Based on proxies of such hydroclimate observations, different drought indices have been proposed and widely used (e.g., Fung, Huang, & Koo, 2020a; Tirivarombo, Osupile, & Eliasson, 2018; Xu, Ren, Ruan, Liu, & Yuan, 2012; Zhai et al., 2010), *e.g.*: i) the Standardized Precipitation Index (SPI; McKee et al., 1993); ii) the Standardized Precipitation minus Evapotranspiration Index (SPEI; Vicente-Serrano et al., 2010); iii) the Palmer Drought Severity Index (PDSI; Palmer, 1965). Comparisons between the SPI, which only considers changes in precipitation, and the SPEI, which includes ET in its calculation, allow for including the effect of warming temperature in considering the shifts of drought conditions (e.g., Stagge, Kingston, Tallaksen, & Hannah, 2017; Tirivarombo et al., 2018; Vicente-Serrano et al., 2010). However, both the SPI and the SPEI do not account for soil moisture content that plays an important role in drought formations (Yoon, Mo, & Wood, 2012). Thus, a more comprehensive drought index, the PDSI, based on the water balance by considering precipitation, temperature, and soil moisture (Heim, 2002; Niemeyer, 2008), has been usually used to serve as a comparison to the SPI or SPEI in drought analysis (e.g., Liu et al., 2013; Sun et al., 2018; Zhai et al., 2010; Zhao et al., 2017). Moreover, the SPI and SPEI both allow for depiction of short-term and multi-year droughts, while the PDSI is more effective for capturing the droughts for a given location and time, making it less flexible for the identification of different time-scaled droughts (Zhao et al., 2017). Considering

their advantages and drawbacks, those drought indices are thus usually used together for drought monitoring.

While drought indices are highly depending on precipitation amount, over Peninsular Malaysia, precipitation variability is primarily driven by monsoons (Fung et al., 2020a; Suhaila, Deni, Wan Zin, & Jemain, 2010), which show large variability from one year to another in response to changes in ocean-atmospheric modes of climate variability (Albani, Ibrahim, & Yong, 2018; Supari et al., 2018; Tangang et al., 2012). The hydroclimate variability over Malaysia has been found to be affected by sea surface temperature (SST) variability, especially over the Pacific Ocean (e.g., Daud, Akhir, & Muslim, 2019; Salimun, Tangang, Juneng, Behera, & Yu, 2014; Suhaila et al., 2010; Tangang & Juneng, 2004) and the Indian Ocean (e.g., Tan, Ibrahim, Cracknell, & Yusop, 2017; Tangang et al., 2012; Tangang et al., 2008). Furthermore, in both the Pacific and Indian oceans, SST variability has been linked to processes modulating the moisture distribution in the troposphere (Chakraborty, Behera, Mujumdar, Ohba, & Yamagata, 2006; Lee, Worden, Noone, Chae, & Frankenberg, 2015; Pillai & Mohankumar, 2010). However, very little is known about the role of the quasi-biennial oscillation (QBO) in triggering droughts in tropical regions, although the QBO was found to affect SST anomalies in the Pacific Ocean, and the Indian summer monsoon rainfall in tropical regions (Chattopadhyay & Bhatla, 2002). Furthermore, it remains unclear how those modes of climate variability in the Pacific and Indian Oceans, and their interactions, influence the mechanisms driving regional water balance, and what their roles are on temporal persistence (i.e. short and long-term drought) and spatial differences of droughts in Asian tropical regions.

The drought conditions over Peninsular Malaysia have been explored in recent studies, but these studies provide inconsistent results using different drought indices (Fung et al., 2020a; Fung, Huang, & Koo, 2020b). Using the SPI, Fung et al. (2020a) suggested that the annual number of dry months was reduced between 1983 and 2017 over most regions of Peninsular

Malaysia. However, Fung et al. (2020b) reported that the occurrence of seasonal droughts (number of dry seasons) increased from 1983 to 2017 over Peninsular Malaysia based on the SPEI. Such inconsistency in previous studies highlight the need to consider multiple drought indices in impact assessment study. Here, we examine spatio-temporal drought conditions in Peninsular Malaysia based on three drought indices, and using four different time scales (i.e., 3-, 6-, 12-, and 24-month). Moreover, we go beyond previous studies (Fung et al., 2020a; Fung et al., 2020b), by examining the relationships between drought conditions and large-scale climatic oscillations, including the QBO and SST variations in the Pacific and Indian oceans, and their relations with regional monsoons. This paper is organised as follows. In Section 2, the general hydrological characteristics of Peninsular Malaysia are summarized, and different data and methods for quantifying drought patterns and climate impacts are presented. In Section 3 and 4, the spatio-temporal drought conditions over Peninsular Malaysia are analysed, and how Peninsular Malaysia drought conditions interact with the regional circulations related to the Pacific and Indian oceans is investigated and discussed. In Section 5, we discuss the potential implications and possible future applications of our results in drought analysis in tropical regions.

2. Materials and Methods

2.1 Study Area

Peninsular Malaysia is characterized by humid and hot climate, with high mean annual rainfall (~2500 mm) and warm temperature (~26°C) throughout the year (Tan, Ibrahim, Duan, Cracknell, & Chaplot, 2015). Due to the weak temperature gradient in the tropic, the climate conditions are somewhat uniform for the whole region. However, Malaysian climate has strong seasonal variations in rainfall, in response to regional monsoon conditions (Fung et al., 2020a; Suhaila et al., 2010). The northeast monsoon (NEM) starts with a wet phase from December to mid-January, bringing heavy rainfall to Malaysia, and this season is then followed by a dry

phase from late January to early March (Tan & Santo, 2018). The southwest monsoon (SWM; June to September) brings less rainfall, as compared to the NEM (Suhaila et al., 2010). In Peninsular Malaysia, the mountains in Main Range (i.e., Banjaran Titiwangsa) separate the West and East of the Peninsular (Suhaila et al., 2010), which affects the water distribution over the region. Based on geographical characteristics defined in Fung et al. (2020), we investigate the spatial hydroclimate conditions of four regions of Peninsular Malaysia (Figure 1): East, South, North, and Central.

2.2 Data

2.2.1 Drought indices

To quantify drought events, three drought indices are used: the SPI (McKee et al., 1993), the SPEI (Vicente-Serrano et al., 2010), and the PDSI (Palmer, 1965). The SPI is suitable for quantifying most types of drought events (Sun et al., 2018), but emphasizes on precipitation amount, unlike the SPEI, which emphasizes the impact of temperature as well (Vicente-Serrano et al., 2010). The SPI is calculated by standardizing precipitation following a Gamma distribution function. Similarly, the SPEI calculation standardizes the precipitation minus the potential evapotranspiration (PET), using a log-logistic distribution function. We use four time scales to capture both short-term (i.e. with a duration no more than a year) and long-term droughts (i.e., lasting more than a year) in the SPI and SPEI: 3-month, 6-month, 12-month and 24-month. In addition, we use the PDSI, which is a comprehensive index considering precipitation, temperature, and soil moisture content (Niemeyer, 2008). However, the conventional PDSI calculation by Palmer (1965), based on the empirical constants for the climatic characteristics of the middle parts of the United States (US), is not suitable for drought quantification in other areas (Wells, Goddard, & Hayes, 2004). Therefore, the self-calibrating PDSI (scPDSI; Wells et al., 2004) is used in this study. For the scPDSI, the empirical constants are adjusted with dynamically calculated values over the interested region. For simplicity, in

following sections, we refer to the scPDSI as the PDSI. In addition, to further investigate droughts over Peninsular Malaysia, five drought levels of the three drought indices are defined (Table 1), and are ranging from no drought (D0) to extreme drought (D4), according to Sun et al. (2018).

Hydroclimatic variables for the three drought indices are extracted from the ERA5-Land monthly averaged dataset (http://doi.org/10.24381/cds.68d2bb30), ranging from 1981 to 2019, at monthly time step (Muñoz, 2019). The ERA5-Land reanalysis dataset has enhanced the spatial resolution of 0.1×0.1°, as compared to the ERA5 dataset (0.25×0.25°). The ERA5-land reanalysis dataset is compared to the observed precipitation data from Kuala Krai station (northern part, 5.53°N, 102.20°E) and Senai station (southern part, 1.63°N, 103.57°E) to evaluate the suitability of the reanalysis data to the region. Generally, the ERA5-land dataset is suitable for the region, as the reanalysis data and observed precipitation match well, with correlations of 0.86 (Kuala Krai station) and 0.72 (Senai station), respectively (Figure A1).

2.2.2 Climate Data

To investigate the underlying climate drivers of drought conditions over Peninsular Malaysia, oceanic indices for the Pacific and Indian oceans have been used, together with an atmospheric oscillation index. The oceanic indices are derived from the extended reconstructed SST version 5 (ERSST.v5) of the National Climate Data Centre (http://doi.org/10.7289/V5T72FNM) (Huang et al., 2017). The main advantage of ERSST.v5 is that this product is not affected by systematic cold SST bias induced by the use of satellite observations at the end of the twentieth century (Reynolds et al. 2002). The ENSO index is calculated based on empirical orthogonal function (EOF) of SST anomalies (SSTa) over the tropical Pacific Ocean (30°S-30°N; 110°E-95°W). This region has been deemed to be able to capture an optimal representations of the ENSO canonical pattern (Dieppois, Rouault, & New, 2015). The Dipole Mode Index (DMI) is

commonly used for assessing the climate variability of the Indian Ocean (Biswas & Kundu, 2018; Harapan et al., 2020; Ibnu Khaldun, Wirasatriya, Dwi Suryo, & Kunarso, 2018). However, based on relative importance analysis, the South Western Indian Ocean (SWIO) is found to explain a larger part of the SPI variance in Peninsular Malaysia than any other indices in the Indian Ocean (Figure A2). Therefore, to avoid redundancy and to overcome issues related to overfitting linear regression models, we only consider the SWIO in this study. As defined in Washington and Preston (2006), the SWIO index is the SSTa average over the south-west Indian Ocean (32°S-25°S, 35°E-90°E).

In tropical Asia regions, such as Malaysia and Singapore, the QBO has been demonstrated to be associated with several tropical surface climate variability, such as the ENSO (Geller, Zhou, & Yuan, 2016; Liess & Geller, 2012) and Indian monsoon rainfall (Fasullo, 2004). As a stratosphere oscillation, the QBO refers to the downward propagating patterns of easterly and westerly zonal winds in the equatorial stratosphere with a period around 25-28 months (Marshall & Scaife, 2009). In this study, the QBO index is calculated from the zonal average of the 30mb zonal wind at the equator (Huang, Hu, Kinter, Wu, & Kumar, 2012), using the 0.25×0.25° ERA-5 reanalysis database (http://doi.org/10.24381/cds.f17050d7), between 1981 and 2019 (Hersbach et al., 2019). To further investigate regional circulations associated with different climate indices, vertically integrated moisture flux divergence and water vapour flux data are extracted from the ERA5 dataset.

2.3 Methods

A diagram outlining the methods for data processing and analysis is shown in Figure 2. The detailed information for these methods are described in following sections.

2.3.1 Trend detection

Using multiple drought indices, we first identify potential temporal trends using a non-parametric Mann-Kendall test (Kendall, 1975; Mann, 1945). However, as it is recognised that the MK trend test can be unreliable if serial-correlations are ignored (Hamed, 2008; Khaliq, Ouarda, & Gachon, 2009), we use a modified MK test, accounting for serial-correlation (Hamed & Ramachandra Rao, 1998). In addition, trend slopes are estimated through Thiel-Sen's slope, which provides a better estimate in the presence of outliers (Sen, 1968).

2.3.2 Identifying spatio-temporal drought patterns

To explore the spatio-temporal drought patterns over Peninsular Malaysia, principal component analysis (PCA) is used (e.g., Awange et al., 2014; Rieser, Kuhn, Pail, Anjasmara, & Awange, 2010). Spatio-temporal gridded datasets (X), describing three drought indices, are decomposed into EOF modes and principal components (PCs), representing the spatial and temporal variations, respectively. It can be written as:

$$X = SP^T \tag{1}$$

where the columns of S and P represent the spatial EOF modes and corresponding temporal PCs, respectively. P^T is the transposition of matrix P. The first three largest EOFs/PCs are usually selected, as they can grasp the main characteristics of original signals and reduce the complexity of original dataset (Awange et al., 2011). However, PCA sometimes may lead to the confusion of spatial patterns, thus causing the difficulty in providing physical interpretations (Hannachi, 2007). Therefore, varimax rotation procedure, one of the most popular rotation method, is applied to EOF modes (hereafter called REOF; Kaiser, 1958; Lian & Chen, 2012) in this study.

2.3.3 Generalised least square (GLS) regressions

The ENSO, SWIO and QBO indices are then used to develop empirical models for drought indices, based on the generalised least square (GLS) regression, for drought indices. These models account for serial correlations, and can be expressed as follows

$$Y = \beta_0 + \beta_1 ENSO + \beta_2 SWIO + \beta_3 QBO + \varepsilon$$

or, more compactly, as (Chandler & Scott, 2011)

$$\boldsymbol{Y} = \boldsymbol{X\beta} + \boldsymbol{\varepsilon} \tag{2}$$

where $\boldsymbol{Y}$ represent the drought indices, and $\boldsymbol{\beta}$ is a 4×1 vector representing the regression coefficients for climate modes of variability $\boldsymbol{X} = (\mathbf{1} \quad \boldsymbol{ENSO} \quad \boldsymbol{SWIO} \quad \boldsymbol{QBO})$. ε is the model errors.

The explicit expression of least squares estimators can be written as

$$\widehat{\boldsymbol{\beta}} = \left(\boldsymbol{X}'\boldsymbol{X}\right)^{-1}\boldsymbol{X}'\boldsymbol{Y} \tag{3}$$

To account for serial correlation, the errors are adjusted by the covariance matrix of $\widehat{\boldsymbol{\beta}}$, as

$$\left(\boldsymbol{X}'\boldsymbol{X}\right)^{-1}\boldsymbol{X}'\widehat{\boldsymbol{\Sigma}}\boldsymbol{X}\left(\boldsymbol{X}'\boldsymbol{X}\right)^{-1} \tag{4}$$

where $\widehat{\boldsymbol{\Sigma}}$ is the estimate of the covariance matrix of errors $\boldsymbol{\varepsilon}$. Suppose the errors are generated using a first-order autoregressive process or AR(1)

$$\varepsilon_t = \phi\varepsilon_{t-1} + \delta_t \tag{5}$$

where $|\phi| < 1$ and δ_t is a white noise sequence. $\widehat{\boldsymbol{\Sigma}}$ can be obtained using estimated parameter $\hat{\phi}$. Thus, adjusted errors can be obtained as the square roots of the diagonal elements of the covariance matrix of $\widehat{\boldsymbol{\beta}}$. Such GLS regression has also been used to investigate the impacts of climate indices on the regional atmospheric circulations. The statistical significance of the GLS regression coefficients is tested based on asymptotically normal tests.

2.3.4 Wavelet transform coherence (WTC)

To investigate climate impacts on droughts at multiple time scales, the wavelet transform coherence (WTC) is used (e.g., He et al., 2020; Torrence & Webster, 1999). Wavelet coherence evaluates the level of linear correlation between two time series *Y* (e.g., the SPI-6 PC1, PC2 and PC3) and *Z* (e.g., the ENSO, SWIO and QBO) at time *n* and on a variability scale *s*. The WTC is then calculated as:

$$R_n^2(Y,Z) = \frac{\left|M\left(s^{-1}W_n^{YZ}(s)\right)\right|^2}{M\left(s^{-1}\left|W_n^Y(s)\right|^2\right)\cdot M\left(s^{-1}\left|W_n^Z(s)\right|^2\right)} \quad (6)$$

where M is a smoothing operator. $W_n^Y(s)$ and $W_n^Z(s)$ are the continuous wavelet transform (CWT) of two time series *Y* and *Z* of length N (i.e., 468 in this study; n=1, 2, …, N), respectively. $W_n^{YZ}(s)$ is the cross-wavelet spectrum, defined as:

$$W_n^{YZ}(s) = W_n^Y(s)W_n^Z(s)^*$$

where $*$ represents the complex conjugate. The significance level of WTC is calculated against red-noises, using 1000 Monte Carlo simulations.

3. Results

3.1 Trend patterns over Peninsular Malaysia

Between 1981 and 2019, both the SPI and SPEI show a tendency toward wetter conditions over most regions of Peninsular Malaysia and at each time scale (Figure 3a-h). Drier conditions, however, emerge locally in the northernmost regions of peninsular (Figure 3a-h). The PDSI also shows a significant trend toward wetter conditions over most Peninsular Malaysia (Figure 3i). Over northern regions of East Peninsular Malaysia, the PDSI shows a tendency toward drier conditions (Figure 3i).

3.2 Temporal changes in drought spatial extensions over Peninsular Malaysia

3.2.1 PDSI vs. SPI/SPEI variations

Section 3.1 shows the differences in spatial trend patterns between the PDSI and the SPI/SPEI. In this section, the temporal similarities and differences between the PDSI and the SPI/SPEI are further examined by regionally averaging variations at different time scales over the whole Peninsular Malaysia. The temporal variability of the PDSI matches well with those of the SPI and the SPEI, especially at 6-month time scale (Figure 4; Table 2). These results indicate that the PDSI is preferred at capturing droughts over a 6-month period. In the following sections, the 6-month SPI and SPEI (i.e. SPI-6 and SPEI-6) have thus been used for further comparison with the PDSI.

3.2.2 Spatial extension of drought in Peninsular Malaysia

Trend analysis indicates that most regions of Peninsular Malaysia are becoming wetter between 1981 and 2019 (cf. Section 3.1). Here, we further examine the spatial extension of drought by evaluating the percentages of area impacted by droughts, based on the SPI-6, SPEI-6, and PDSI (Figure 5). The SPI-6, SPEI-6, and PDSI show very similar pattern, suggesting that, between 1981 and 2019, Peninsular Malaysia experienced several severe droughts (Figure 5): 1981-1983, 1987, 1992, 1998, 2003-2005, and 2015-2016. Interestingly, these droughts occur at the same time as El Nino episodes (Figure A3). Among these droughts, the droughts in 1983 and 2005 were the most severe in terms of the spatial extension and duration based on all drought indices (Figure 5). In 1983 and 2005, almost the whole Peninsular Malaysia experienced a certain degree of droughts (i.e., from mild drought to extreme drought), and around 60% (in 1983) and 30% (in 2005) of the region suffered from extreme drought (Figure 5). However, compared with the SPI/SPEI, the PDSI indicates higher severity and larger spatial extension for drought events in 1987 and 1992, which have been reported as severe droughts that cover the whole Peninsular Malaysia (Cheang, 1993; Tan et al., 2020; UNWATER, 2014). To further

explore the spatial drought severity and spatial extension in these years, the spatial patterns of precipitation deficits in 1983, 1987, 1992 and 2005 are shown in Figure 6. Consistent with drought percentage results of three drought indices, almost the whole Peninsular Malaysia experienced droughts in 1983 and 2005 (Figure 6a and 6d). The drought severity also showed spatial differences: the drought was more severe in the North and Central regions compared to other regions (Figure 6a and 6d). However, there were positive precipitation deficits (wetting) over almost the whole Peninsular Malaysia in 1987 (Figure 6b). In 1992, precipitation deficit map indicates South and Central region were becoming wetter, while East and North part were becoming slightly drier (Figure 6c). The 1987 and 1992 severe droughts (Tan et al., 2020; UNWATER, 2014), are detected by the PDSI, but their severity are not well presented in the SPI/SPEI. Therefore, the PDSI is much more reliable than the SPI/SPEI by considering more variables.

In addition, we note that drought is becoming less severe and less widespread between 1981 and 2019 over Peninsular Malaysia based on all drought indices (Figure 5), which is consistent with wetter conditions, as indicated by trend analysis (Figure 3). Even though the whole Peninsular Malaysia is becoming wetter at a long-term scale, the study region can still suffer from severe droughts over short periods (i.e., 1-2 years). Therefore, exploring spatio-temporal patterns of droughts and their connections with climate variability are still necessary over Peninsular Malaysia for future regional hazard prevention and water management.

3.3 Spatio-temporal modes of variability for drought over Peninsular Malaysia

To further explore the drought spatio-temporal variability over Peninsular Malaysia, the first three REOFs of the SPI (i.e., SPI-REOF1, SPI-REOF2, and SPI-REOF3) are extracted for different time scales (Figure 7).

Representing around 60% of the total variance of the SPI, the REOF1 is the main modes of spatio-temporal drought variability, showing a North-South (N-S) gradient, with alternating dry (wet) conditions in the North and Central part, but wet (dry) conditions in the South and East (Figure 7a-d). The temporal variations of the SPI-PC1 are strongly correlated to the average SPI variations over Peninsular Malaysia, with correlation values reaching -0.97, at p-value < 0.05, for all time scales (Figure A4). The SPI-REOF2 and -REOF3 express much lower fractions of spatio-temporal variance of drought across Peninsular Malaysia (~13% and 7%, respectively; Figure 7e-l). However, these two REOFs allow for examining background spatio-temporal variations, which could not be detected using the regionally averaged SPI over the region, as it is not significantly correlated to the SPI-PC2 and -PC3 (Figure 7). The SPI-REOF2 shows homogeneous dry or wet conditions, but the dry (or wet) intensities are much stronger in the northern part than southern part, which can be also seen as a N-S gradient (Figure 7e-h). The SPI-REOF3 refers to alternating dry (wet) conditions over the western regions of Peninsular Malaysia, while wet (dry) conditions occur in the eastern regions (hereafter called East-West [E-W] gradient; Figure 7i-l).

Combining three modes of the SPI allows to identify four different regions with consistent spatio-temporal variations of drought (Figure A5): East, North, South, and Central part of Peninsular Malaysia. Note that similar modes of spatio-temporal drought variability are found using the SPEI over Peninsular Malaysia (Figure A6). For the PDSI, although three REOFs only explain around 50% of total variances, they also indicate spatial differences between South (West) and North (East), consistent with the SPI patterns (Figure A7).

3.4 Underlying climate mechanisms driving drought conditions

3.4.1 Regional drought variations and large-scale climate variability

To explore the underlying climate drivers of drought conditions over Peninsular Malaysia, Figure 8 displays the regression maps between the ENSO, SWIO, QBO, and the SPI.

The ENSO and SWIO show significant negative relationships with the SPI variations over most Peninsular Malaysia, while the QBO shows positive relationships (Figure 8). This suggests that the warm phases of the ENSO (i.e. El Nino) and the SWIO favour droughts over the whole region, while the positive QBO (i.e. more stratospheric easterly winds) alleviates drought conditions. Moreover, eastern region is generally much drier than other parts of Peninsular Malaysia during El Nino years, indicating the spatial differences in the ENSO impacts (Figure 8a-d). Similarly, the impacts of the SWIO on droughts over Peninsular Malaysia are stronger in the southern region than in the northern region (Figure 8e-h). The QBO impacts are generally much stronger in the eastern peninsular compared to the western part (Figure 8i-l). We also note that the strength of the impacts of climate drivers on droughts varies among different time scales (Figure 8). The ENSO impacts on droughts are stronger at 6- and 12-month time scales (Figure 8a-d). The SWIO contributions to droughts are more pronounced on longer time scales (e.g., 24-month; Figure 9e-h), while the QBO impacts are stronger at 12-month time scale (Figure 8i-l). In summary, spatially, the N-S and E-W gradients showed in the SPI-REOFs may be attributed to the spatial differences in impacts of the ENSO, SWIO, and QBO on droughts. In addition, the ENSO and QBO may affect more for droughts lasting a year or less, while the SWIO has a stronger impact on longer-term or multi-year drought conditions (i.e., 2 years or more).

To examine the contribution of warming temperature to droughts, we examine the same regression maps, but using the SPEI (Figure 9). As for the SPI, the ENSO and SWIO have significant negative impacts on the SPEI over the most peninsular Malaysia, while the QBO has positive effects (Figure 9). However, compared to the SPI, the impacts of the ENSO, SWIO and QBO on the SPEI strengthen. Such strengthening in the impacts of the ENSO, SWIO, and QBO on droughts over Peninsular Malaysia suggests a significant role of such modes of climate variability on temperature and evapotranspiration, enhancing their impacts on droughts. The

same regressions, but using the PDSI, show similar impact strengthening patterns (Figure 10), confirming the impacts of rising temperature and evapotranspiration on droughts over Peninsular Malaysia.

3.4.2 Time-scale dependence of links between drought spatio-temporal variations and large-scale climate variability

Section 3.4.1 suggests spatial differences in the impacts of large-scale climate variability on droughts, and its persistence (i.e., short-term and long-term drought). We here examine how the relationship between climate indices and drought spatio-temporal variations (REOF1 to 3) evolve over time, and at different time scales, using the WTC (Figure 11).

The WTC analysis between the ENSO and the SPI6-PC1 (i.e. the N-S gradient in drought conditions) reveals a strong relationship, specifically centered on 4-year time scale (Figure 11a). We also note that the time lag (i.e., phase lag) for the relationship between the ENSO and the SPI6-PC1 is changing over time, from 0.5 year during 1981-1990 to 0 year during 1991-2019 on 4-year time scale (Figure 11a). Similarly, the relationship between the SPI6-PC1 and the SWIO is only significant, and particularly pronounced, on 4-8 year time scales, with a time lag around 1-2 years (Figure 11b). The QBO impacts on the SPI6-PC1 are much weaker, but centered on high-frequency time scales (≤2 years; Figure 11c). The ENSO shows a strong relationship with the SPI6-PC2, which also represents a N-S gradient in drought conditions (Figure 11d). Such relationship is mainly on 2-4 year time scale, with a time lag around 0.5-1 year (Figure 11d).

The timing of the ENSO impacts on the SPI6-PC1 (~4 years) and -PC2 (2-4 years) is however different, suggesting the interannual changes in the relationship between the ENSO and drought spatio-temporal variability over Peninsular Malaysia (Figure 11a, d). Moreover, the impacts of the SWIO on the SPI6-PC2 (i.e., the N-S gradient in drought conditions) are significant on 4-year time scale between 2000 and 2010, but much weaker than that on the SPI6-PC1 (Figure

11e). For the SPI6-PC3 (i.e. the E-W gradient in drought conditions), the impacts of the ENSO and SWIO are generally much weaker than on the SPI6-PC1 and -PC2 (Figure 11g-h). However, the QBO shows significant impacts on the SPI6-PC3 at 2-year time scale, much stronger than that on the SPI6-PC1 and-PC2 (Figure 11c, f, i).

Altogether, the results indicate that both the ENSO and SWIO contribute to more or less pronounced the N-S gradient in drought conditions over Peninsular Malaysia. Likewise, the QBO has a stronger impact on the E-W gradients in drought conditions over Peninsular Malaysia.

3.4.3 Mechanisms driving climate-drought teleconnections in Peninsular Malaysia

Here, we examine the regional circulation associated with the ENSO, SWIO, and QBO to identify the mechanisms of large-scale processes leading to the spatio-temporal variability in droughts over Peninsular Malaysia. Figure 12 shows the regressed surface atmospheric moisture flux associated with the ENSO, SWIO, and QBO, and their relations to the SWM in boreal summer (JJA) and the NEM in boreal winter (DJF).

During JJA, the SWM wind brings heavy moisture to the western coast of the Indochinese Peninsula and the western part of Peninsular Malaysia, while other parts of the peninsular have relatively low precipitation (Figure 12a). In boreal summer, the ENSO has significant positive impacts on moisture flux divergence over Peninsular Malaysia (Figure 12b), indicating that El Nino events favour the export of continental moisture toward the ocean, reducing precipitable water over land. Warmer SWIO seems to promote northeasterly/easterly moisture flux, weakening the SWM wind, and favouring precipitation deficits over the western part of Peninsular Malaysia (Figure 12c). Over Peninsular Malaysia, the positive QBO promotes westerly moisture flux, as well as moisture convergence over land, favouring more precipitation (Figure 12d). In boreal winter (DJF), the NEM wind brings precipitation to the

eastern part of Peninsular Malaysia (Figure 12e). During that season, the warm phases of the ENSO and SWIO significantly weaken the NEM winds, favouring droughts as a response of precipitation deficits over the peninsula (Figure 12f-g). The QBO impacts are statistically non-significant in DJF (Figure 12h).

In summary, the ENSO, SWIO, and QBO are related to the SWM and NEM winds, and contribute to precipitation deficits and droughts over the peninsula. Their impacts on droughts largely contribute to the differences between northern and southern regions, as well as eastern and western regions. These spatial differences may, however, partly be attributed to the geographic characteristics, as the Main Range Mountains separate the western and eastern parts of the peninsular (Suhaila et al., 2010), and mountains in the northeastern region (Figure 1) also separate the northern and southern part. The SWM in JJA brings moistures to western coast of peninsular, and the mountains prevent moisture from entering the eastern part. The QBO brings more precipitation by enhancing the SWM, which combined with orographic effects, explains why the QBO is associated with the E-W gradient in drought conditions over Peninsular Malaysia. Similarly, during DJF, the ENSO and SWIO weaken the NEM, which interact with mountains in the northeastern region (Figure 1), and lead to the N-S gradient in precipitation deficits.

4. Discussion

4.1 Difference of three drought indices for drought analysis

Previous studies have suggested that different drought indices may get different results over the same region and during the same period (e.g., Fung et al., 2020a; Fung et al., 2020b). Fung et al. (2020a) showed an increase of annual precipitation, and a decreasing number of drought events, except in the Southern region between 1983 and 2017 based on the SPI. However, the SPEI analysis suggested that both the occurrence of seasonal droughts and the number of dry

seasons had increased during 1983-2017 (Fung et al., 2020b). In our study, similar inconsistency among different drought indices for long term trend analysis over Peninsular Malaysia are found. Despite a significant increase in the SPI and SPEI over northern part of East Peninsular Malaysia (Figure 3a-d), these regions are becoming drier according to the PDSI (Figure 3i). Such discrepancy between the SPI/SPEI and the PDSI is likely caused by the different foundations of the indices. The PDSI is a comprehensive drought index integrating precipitation, temperature, and soil moisture, while the SPI (and SPEI) only considers the precipitation (and temperature) variations. Sheffield, Wood, and Roderick (2012) however suggested that the influences of warming temperature on droughts are likely to be overestimated based on the PDSI calculations. Therefore, compared to the SPI and SPEI, which detect drying conditions in a very small part, the PDSI may expand the drying conditions due to an overestimation of the effect of rising temperature. In addition, soil moisture variations are related to topographic elements and land use (Guo et al., 2020; Yang, Dou, Liu, & An, 2017). The drying regions detected by the PDSI are the mountainous areas, whereas wetting regions are lowland areas (Figure 1). Thus, the different land uses may affect the drought conditions, leading to the observed differences between the PDSI and the SPI/SPEI.

4.2 Underlying climate mechanism of drought patterns over Peninsular Malaysia

From 1981 to 2019, droughts are less severe and less widespread over Peninsular Malaysia, which is regulated by the ENSO, SWIO and QBO through the modulations of the SWM and NEM winds. During El Nino episodes, the warm phases of the SWIO, and the westerly phase of the QBO, droughts are more likely to strike the peninsula. The impacts of the ENSO on water variability over Malaysia are consistent with previous studies (e.g., Juneng & Tangang, 2005; Salimun et al., 2014; Tangang & Juneng, 2004). The SST variability in Indian Ocean (IOD) and tropical atmosphere oscillations (i.e., Madden-Julian Oscillation [MJO]) are also suggested to affect the hydroclimate variability over Peninsular Malaysia (Islam, Chan,

Ashfold, Ooi, & Azari, 2018; Tangang et al., 2008), even though the specific climate indices are different from those in our study. Our statistical analysis suggests that the SWIO has larger contributions to drought conditions compared to the IOD (Figure A2). The MJO and the QBO are two key modes of variability in the tropical atmosphere, both affecting the tropical convection (Islam et al., 2018; Liess & Geller, 2012). However, the MJO normally weakens when it approaches the Malaysia region (Zhang, 2013). Therefore, the QBO should be a better choice of tropical atmosphere oscillations for affecting local water variability over Peninsular Malaysia compared to the MJO. In addition, there are interactions among the ENSO, Indian SST variability and QBO (Pillai & Mohankumar, 2010), and we need further investigations for the interaction of these oscillations, similarly to previous studies for studying relations between the ENSO and the SWIO (Cai et al. 2011; Weller; Cai 2013), and between the ENSO and the QBO (Calvo et al. 2009; Hansen et al. 2015).

5. Conclusions

Using three drought indices from 1981 to 2019, we analyse the spatio-temporal drought patterns over Peninsular Malaysia at four time scales (i.e., 3-, 6-, 12-, and 24-month). Over the past decades, there is generally a significant tendency toward wetter conditions over the region, based on all drought indices (i.e. the SPI, SPEI, and PDSI). Moreover, based on the analysis of interannual changes in the drought severity and drought spatial extensions, results indicate that, from 1981 to 2019, droughts are less severe and less widespread over Peninsular Malaysia, but the region still suffered severe droughts during past decades, like 1983 and 2005. Based on the PCA results, generally, the first and second mode of drought spatio-temporal variability reveal the N-S gradient of drought conditions over Peninsular Malaysia, while the third mode indicates the E-W differences in droughts.

To characterise how large-scale ocean-atmosphere oscillations are related to drought conditions, the GLS models have been used to establish the relationships between drought

indices and three climate indices: the ENSO, SWIO, and QBO. All three indices are found to be linked to drought conditions, via modulations of the SWM and NEM winds. Droughts are more likely to occur over the peninsula during the El Nino events, the warm phases of the SWIO and the westerly phases of the QBO. Moreover, those modes of large-scale climate variability show stronger impacts on droughts using the SPEI and PDSI, rather than the SPI. It indicates that those climate oscillations may affect the local temperature and evapotranspiration, exacerbating drought patterns over Peninsular Malaysia.

Additionally, the response of drought patterns to the ENSO and SWIO largely contributes to differences between the North and South, while the impacts of the QBO may contribute more to the E-W differences. These spatial differences may, however, be related to interactions between the large-scale atmospheric circulations and the orographic factors over the region. For instance, moisture fluxes associated with the SWM in JJA, and the NEM in DJF, are prevented from spreading throughout the peninsular by the mountains. In addition, the ENSO and QBO show stronger impacts on droughts lasting a year or less, while the SWIO is associated with multi-year droughts (i.e. ≥2 years).

Based on the above results, despite that Peninsular Malaysia recorded a tendency toward wetter conditions, we show that, from one year to another, some regions may still suffer from droughts due to the interactions between large-scale atmospheric circulations and orographic factors. Local stakeholders may need to pay more attention to such regional droughts in the future. In particular, warming ocean temperature, especially in the Indian and Pacific oceans, might contribute to increase drought risks over Peninsular Malaysia (Cai et al., 2014; Chu et al., 2018). The expected future risks in droughts could thus put more pressure on the local Malaysian Government for water supply and food security. Overall, the empirical relationships between drought conditions over Peninsular Malaysia and the atmosphere-ocean oscillations linked with

monsoon circulations can be valuable to develop seasonal to multi-year empirical forecast for water resources management in tropical Asia.

Acknowledgement

This study was supported by the Scientific and Technological Research Council of Turkey (TUBITAK) 2232 grant (118C329). The study also funded by the Ministry of Higher Education Malaysia under the Fundamental Research Grant Scheme (203.PHUMANITI.6711695). This research was conducted using the resources of the High Performance Cluster Computing Centre, Hong Kong Baptist University, which receives funding from Research Grant Council, University Grant Committee of the HKSAR and Hong Kong Baptist University. The drought approach in the paper was developed from the PROCORE-France/Hong Kong Joint Research Scheme 2020/21 (F-HKBU201/20).

Data Availability Statement

The station data that support the findings of this study are available on request from the co-author. The data are not publicly available due to privacy or ethical restrictions. The other data that support the findings of this study are openly available in **ERA5-Land monthly averaged data from 1981 to present** at http://doi.org/10.24381/cds.68d2bb30 (Muñoz, 2019), **ERA5 monthly averaged data on single levels from 1979 to present** at http://doi.org/10.24381/cds.f17050d7 (Hersbach et al., 2019), NOAA Extended Reconstructed Sea Surface Temperature (ERSST), Version 5 at http://doi.org/10.7289/V5T72FNM (Huang et al., 2017).

References

Albani, A., Ibrahim, M. Z., & Yong, K. H. (2018). Influence of the ENSO and Monsoonal Season on Long-Term Wind Energy Potential in Malaysia. *Energies, 11*(11). doi:10.3390/en11112965

Awange, J. L., Fleming, K. M., Kuhn, M., Featherstone, W. E., Heck, B., & Anjasmara, I. (2011). On the suitability of the 4°×4° GRACE mascon solutions for remote sensing Australian hydrology. *Remote Sensing of Environment, 115*(3), 864-875. doi:https://doi.org/10.1016/j.rse.2010.11.014

Awange, J. L., Gebremichael, M., Forootan, E., Wakbulcho, G., Anyah, R., Ferreira, V. G., & Alemayehu, T. (2014). Characterization of Ethiopian mega hydrogeological regimes using GRACE, TRMM and GLDAS datasets. *Advances in Water Resources, 74*, 64-78. doi:https://doi.org/10.1016/j.advwatres.2014.07.012

Biswas, H. R., & Kundu, P. K. (2018). A principal component analysis based model to predict post-monsoon tropical cyclone activity in the Bay of Bengal using oceanic Niño index and dipole mode index. *International Journal of Climatology, 38*(5), 2415-2422. doi:https://doi.org/10.1002/joc.5344

Cai, W., Borlace, S., Lengaigne, M., van Rensch, P., Collins, M., Vecchi, G., . . . Jin, F.-F. (2014). Increasing frequency of extreme El Niño events due to greenhouse warming. *Nature Climate Change, 4*(2), 111-116. doi:10.1038/nclimate2100

Chakraborty, A., Behera, S. K., Mujumdar, M., Ohba, R., & Yamagata, T. (2006). Diagnosis of Tropospheric Moisture over Saudi Arabia and Influences of IOD and ENSO. *Monthly Weather Review, 134*(2), 598-617. doi:10.1175/MWR3085.1

Chandler, R. E., & Scott, E. M. (2011). Parametric Modelling – Deterministic Trends. In *Statistical Methods for Trend Detection and Analysis in the Environmental Sciences* (pp. 61-125).

Chattopadhyay, J., & Bhatla, R. (2002). Possible influence of QBO on teleconnections relating Indian summer monsoon rainfall and sea-surface temperature anomalies across the equatorial pacific. *International Journal of Climatology, 22*(1), 121-127. doi:10.1002/joc.661

Cheang, B.-k. (1993). Interannual variability of monsoons in Malaysia and its relationship with ENSO. *Proceedings of the Indian Academy of Sciences - Earth and Planetary Sciences, 102*(1), 219-239. doi:10.1007/BF02839192

Chen, H., & Sun, J. (2015). Changes in Drought Characteristics over China Using the Standardized Precipitation Evapotranspiration Index. *Journal of Climate, 28*(13), 5430-5447. doi:10.1175/JCLI-D-14-00707.1

Chinnasamy, P., & Ganapathy, R. (2017). Long-term variations in water storage in Peninsular Malaysia. *Journal of Hydroinformatics, 20*(5), 1180-1190. doi:10.2166/hydro.2017.043

Chu, C., Yang, X.-Q., Sun, X., Yang, D., Jiang, Y., Feng, T., & Liang, J. (2018). Effect of the tropical Pacific and Indian Ocean warming since the late 1970s on wintertime Northern Hemispheric atmospheric circulation and East Asian climate interdecadal changes. *Climate Dynamics, 50*(7), 3031-3048. doi:10.1007/s00382-017-3790-y

Daud, N. R., Akhir, M. F., & Muslim, A. M. (2019). Dynamic of ENSO towards upwelling and thermal front zone in the east coast of Peninsular Malaysia. *Acta Oceanologica Sinica, 38*(1), 48-60. doi:10.1007/s13131-019-1369-7

Dieppois, B., Rouault, M., & New, M. (2015). The impact of ENSO on Southern African rainfall in CMIP5 ocean atmosphere coupled climate models. *Climate Dynamics, 45*(9), 2425-2442. doi:10.1007/s00382-015-2480-x

Fasullo, J. (2004). Biennial Characteristics of Indian Monsoon Rainfall. *Journal of Climate, 17*(15), 2972-2982. doi:10.1175/1520-0442(2004)017<2972:BCOIMR>2.0.CO;2

Firdaus, R. B. R., Leong Tan, M., Rahmat, S. R., & Senevi Gunaratne, M. (2020). Paddy, rice and food security in Malaysia: A review of climate change impacts. *Cogent Social Sciences, 6*(1), 1818373. doi:10.1080/23311886.2020.1818373

Fung, K. F., Huang, Y. F., & Koo, C. H. (2020a). Assessing drought conditions through temporal pattern, spatial characteristic and operational accuracy indicated by SPI and SPEI: case analysis for Peninsular Malaysia. *Natural Hazards*. doi:10.1007/s11069-020-04072-y

Fung, K. F., Huang, Y. F., & Koo, C. H. (2020b). Spatiotemporal analysis of seasonal SPEI in Peninsular Malaysia. *IOP Conference Series: Earth and Environmental Science, 476*, 012113. doi:10.1088/1755-1315/476/1/012113

Geller, M. A., Zhou, T., & Yuan, W. (2016). The QBO, gravity waves forced by tropical convection, and ENSO. *Journal of Geophysical Research: Atmospheres, 121*(15), 8886-8895. doi:10.1002/2015JD024125

Guo, X., Fu, Q., Hang, Y., Lu, H., Gao, F., & Si, J. (2020). Spatial Variability of Soil Moisture in Relation to Land Use Types and Topographic Features on Hillslopes in the Black Soil (Mollisols) Area of Northeast China. *Sustainability, 12*(9). doi:10.3390/su12093552

Hamed, K. H. (2008). Trend detection in hydrologic data: The Mann–Kendall trend test under the scaling hypothesis. *Journal of Hydrology, 349*(3), 350-363. doi:https://doi.org/10.1016/j.jhydrol.2007.11.009

Hamed, K. H., & Ramachandra Rao, A. (1998). A modified Mann-Kendall trend test for autocorrelated data. *Journal of Hydrology, 204*(1), 182-196. doi:https://doi.org/10.1016/S0022-1694(97)00125-X

Hannachi, A. (2007). Pattern hunting in climate: a new method for finding trends in gridded climate data. *International Journal of Climatology, 27*(1), 1-15. doi:https://doi.org/10.1002/joc.1375

Harapan, H., Yufika, A., Anwar, S., Te, H., Hasyim, H., Nusa, R., . . . Mudatsir, M. (2020). Effects of El Niño Southern Oscillation and Dipole Mode Index on Chikungunya Infection in Indonesia. *Tropical Medicine and Infectious Disease, 5*(3). doi:10.3390/tropicalmed5030119

He, Q., Chun, K. P., Sum Fok, H., Chen, Q., Dieppois, B., & Massei, N. (2020). Water storage redistribution over East China, between 2003 and 2015, driven by intra- and inter-annual climate variability. *Journal of Hydrology, 583*, 124475. doi:https://doi.org/10.1016/j.jhydrol.2019.124475

Heim, J. R. R. (2002). A Review of Twentieth-Century Drought Indices Used in the United States. *Bulletin of the American Meteorological Society, 83*(8), 1149-1166. doi:10.1175/1520-0477-83.8.1149

Hersbach, H., Bell, B., Berrisford, P., Biavati, G., Horányi, A., Muñoz Sabater, J., . . . Thépaut, J.-N. (2019). *ERA5 monthly averaged data on single levels from 1979 to present*. Retrieved from: https://cds.climate.copernicus.eu/cdsapp#!/home

Huang, B., Hu, Z.-Z., Kinter, J. L., Wu, Z., & Kumar, A. (2012). Connection of stratospheric QBO with global atmospheric general circulation and tropical SST. Part I: methodology and composite life cycle. *Climate Dynamics, 38*(1), 1-23. doi:10.1007/s00382-011-1250-7

Huang, B., Thorne, P. W., Banzon, V. F., Boyer, T., Chepurin, G., Lawrimore, J. H., . . . Zhang, H.-M. (2017). *NOAA Extended Reconstructed Sea Surface Temperature (ERSST), Version 5*. Retrieved from: https://www.ncei.noaa.gov/access/metadata/landing-page/bin/iso?id=gov.noaa.ncdc:C00927

Hui-Mean, F., Yusof, F., Yusop, Z., & Suhaila, J. (2019). Trivariate copula in drought analysis: a case study in peninsular Malaysia. *Theoretical and Applied Climatology, 138*(1), 657-671. doi:10.1007/s00704-019-02847-3

Ibnu Khaldun, M. H., Wirasatriya, A., Dwi Suryo, A. A., & Kunarso. (2018). The Influence of Indian Ocean Dipole (IOD) on The Variability of Sea Surface Temperature and Precipitation in Sumatera Island. *IOP Conference Series: Earth and Environmental Science, 165*, 012008. doi:10.1088/1755-1315/165/1/012008

Islam, M. A., Chan, A., Ashfold, M. J., Ooi, C. G., & Azari, M. (2018). Effects of El-Niño, Indian Ocean Dipole, and Madden-Julian Oscillation on Surface Air Temperature and Rainfall Anomalies over Southeast Asia in 2015. *Atmosphere, 9*(9). doi:10.3390/atmos9090352

Juneng, L., & Tangang, F. T. (2005). Evolution of ENSO-related rainfall anomalies in Southeast Asia region and its relationship with atmosphere–ocean variations in Indo-Pacific sector. *Climate Dynamics, 25*(4), 337-350.

Kaiser, H. F. (1958). The varimax criterion for analytic rotation in factor analysis. *Psychometrika, 23*(3), 187-200.

Kendall, M. G. (1975). *Rank correlation methods*. Oxford, England: Griffin.

Khaliq, M. N., Ouarda, T. B. M. J., & Gachon, P. (2009). Identification of temporal trends in annual and seasonal low flows occurring in Canadian rivers: The effect of short- and long-term persistence. *Journal of Hydrology, 369*(1), 183-197. doi:https://doi.org/10.1016/j.jhydrol.2009.02.045

Lee, J., Worden, J., Noone, D., Chae, J. H., & Frankenberg, C. (2015). Isotopic changes due to convective moistening of the lower troposphere associated with variations in the ENSO and IOD from 2005 to 2006. *Tellus B: Chemical and Physical Meteorology, 67*(1), 26177. doi:10.3402/tellusb.v67.26177

Li, B., & Rodell, M. (2015). Evaluation of a model-based groundwater drought indicator in the conterminous U.S. *Journal of Hydrology, 526*, 78-88. doi:https://doi.org/10.1016/j.jhydrol.2014.09.027

Lian, T., & Chen, D. (2012). An Evaluation of Rotated EOF Analysis and Its Application to Tropical Pacific SST Variability. *Journal of Climate, 25*(15), 5361-5373. doi:10.1175/JCLI-D-11-00663.1

Liess, S., & Geller, M. A. (2012). On the relationship between QBO and distribution of tropical deep convection. *Journal of Geophysical Research: Atmospheres, 117*(D3). doi:10.1029/2011JD016317

Liu, L., Hong, Y., Looper, J., Riley, R., Yong, B., Zhang, Z., . . . Shafer, M. (2013). Climatological Drought Analyses and Projection Using SPI and PDSI: Case Study of the Arkansas Red River Basin. *Journal of Hydrologic Engineering, 18*(7), 809-816. doi:10.1061/(ASCE)HE.1943-5584.0000619

Mann, H. B. (1945). Nonparametric Tests Against Trend. *Econometrica, 13*(3), 245-259. doi:10.2307/1907187

Marshall, A. G., & Scaife, A. A. (2009). Impact of the QBO on surface winter climate. *Journal of Geophysical Research: Atmospheres, 114*(D18). doi:10.1029/2009JD011737

Martínez-Fernández, J., González-Zamora, A., Sánchez, N., Gumuzzio, A., & Herrero-Jiménez, C. M. (2016). Satellite soil moisture for agricultural drought monitoring: Assessment of the SMOS derived Soil Water Deficit Index. *Remote Sensing of Environment, 177*, 277-286. doi:https://doi.org/10.1016/j.rse.2016.02.064

McKee, T. B., Doesken, N. J., & Kleist, J. (1993). *The relationship of drought frequency and duration to time scales.* Paper presented at the Proceedings of the 8th Conference on Applied Climatology.

Muñoz, S., J. (2019). *C3S ERA5-Land reanalysis*. Retrieved from: https://cds.climate.copernicus.eu/cdsapp#!/home

Munson, S. M., Bradford, J. B., & Hultine, K. R. (2020). An Integrative Ecological Drought Framework to Span Plant Stress to Ecosystem Transformation. *Ecosystems*. doi:10.1007/s10021-020-00555-y

Niemeyer, S. (2008). New drought indices. *Options Méditerranéennes. Série A: Séminaires Méditerranéens, 80*, 267-274.

Nurul Fatin, M., Mohd Razali, S., Ahmad, A. A., & Mohd Shafri, Z. M. S. (2019). Oil palm dry season analysis based on moderate-resolution imaging spectroradiometer (MODIS) satellite indices. *International Journal of Remote Sensing, 40*(19), 7663-7678. doi:10.1080/01431161.2019.1608394

Palmer, W. C. (1965). Meteorological drought. U.S. *Weather Bureau Res. Paper, 45*, 1-58.

Pillai, P. A., & Mohankumar, K. (2010). Individual and combined influence of El Niño–Southern Oscillation and Indian Ocean Dipole on the Tropospheric Biennial Oscillation. *Quarterly Journal of the Royal Meteorological Society, 136*(647), 297-304. doi:https://doi.org/10.1002/qj.579

Rieser, D., Kuhn, M., Pail, R., Anjasmara, I. M., & Awange, J. (2010). Relation between GRACE-derived surface mass variations and precipitation over Australia. *Australian Journal of Earth Sciences, 57*(7), 887-900. doi:10.1080/08120099.2010.512645

Salimun, E., Tangang, F., Juneng, L., Behera, S. K., & Yu, W. (2014). Differential impacts of conventional El Niño versus El Niño Modoki on Malaysian rainfall anomaly during winter monsoon. *International Journal of Climatology, 34*(8), 2763-2774. doi:10.1002/joc.3873

Sanusi, W., Jemain, A. A., Zin, W. Z. W., & Zahari, M. (2015). The Drought Characteristics Using the First-Order Homogeneous Markov Chain of Monthly Rainfall Data in Peninsular Malaysia. *Water Resources Management, 29*(5), 1523-1539. doi:10.1007/s11269-014-0892-8

Sen, P. K. (1968). Estimates of the Regression Coefficient Based on Kendall's Tau. *Journal of the American Statistical Association, 63*(324), 1379-1389. doi:10.1080/01621459.1968.10480934

Sheffield, J., Wood, E. F., & Roderick, M. L. (2012). Little change in global drought over the past 60 years. *Nature, 491*(7424), 435-438. doi:10.1038/nature11575

Shukla, S., & Wood, A. W. (2008). Use of a standardized runoff index for characterizing hydrologic drought. *Geophysical Research Letters, 35*(2). doi:10.1029/2007gl032487

Stagge, J. H., Kingston, D. G., Tallaksen, L. M., & Hannah, D. M. (2017). Observed drought indices show increasing divergence across Europe. *Scientific Reports, 7*(1), 14045. doi:10.1038/s41598-017-14283-2

Suhaila, J., Deni, S. M., Wan Zin, W. Z., & Jemain, A. A. (2010). Spatial patterns and trends of daily rainfall regime in Peninsular Malaysia during the southwest and northeast monsoons: 1975–2004. *Meteorology and Atmospheric Physics, 110*(1-2), 1-18. doi:10.1007/s00703-010-0108-6

Sun, Z., Zhu, X., Pan, Y., Zhang, J., & Liu, X. (2018). Drought evaluation using the GRACE terrestrial water storage deficit over the Yangtze River Basin, China. *Sci Total Environ, 634*, 727-738. doi:10.1016/j.scitotenv.2018.03.292

Supari, Tangang, F., Salimun, E., Aldrian, E., Sopaheluwakan, A., & Juneng, L. (2018). ENSO modulation of seasonal rainfall and extremes in Indonesia. *Climate Dynamics, 51*(7), 2559-2580. doi:10.1007/s00382-017-4028-8

Tallaksen, L. M., & Van Lanen, H. A. (2004). *Hydrological drought: processes and estimation methods for streamflow and groundwater* (Vol. 48): Elsevier.

Tan, L. M., Ibrahim, L. A., Duan, Z., Cracknell, P. A., & Chaplot, V. (2015). Evaluation of Six High-Resolution Satellite and Ground-Based Precipitation Products over Malaysia. *Remote Sensing, 7*(2). doi:10.3390/rs70201504

Tan, M. L., Ibrahim, A. L., Cracknell, A. P., & Yusop, Z. (2017). Changes in precipitation extremes over the Kelantan River Basin, Malaysia. *International Journal of Climatology, 37*(10), 3780-3797. doi:https://doi.org/10.1002/joc.4952

Tan, M. L., Juneng, L., Tangang, F. T., Samat, N., Chan, N. W., Yusop, Z., & Ngai, S. T. (2020). SouthEast Asia HydrO-meteorological droughT (SEA-HOT) framework: A case study in the Kelantan River Basin, Malaysia. *Atmospheric Research, 246*, 105155. doi:https://doi.org/10.1016/j.atmosres.2020.105155

Tan, M. L., & Santo, H. (2018). Comparison of GPM IMERG, TMPA 3B42 and PERSIANN-CDR satellite precipitation products over Malaysia. *Atmospheric Research, 202*, 63-76. doi:https://doi.org/10.1016/j.atmosres.2017.11.006

Tangang, F. T., & Juneng, L. (2004). Mechanisms of Malaysian Rainfall Anomalies. *Journal of Climate, 17*(18), 3616-3622. doi:10.1175/1520-0442(2004)017<3616:MOMRA>2.0.CO;2

Tangang, F. T., Juneng, L., Salimun, E., Sei, K., Le, L., & Halimatun, M. (2012). Climate change and variability over Malaysia: gaps in science and research information. *Sains Malaysiana, 41*(11), 1355-1366.

Tangang, F. T., Juneng, L., Salimun, E., Vinayachandran, P. N., Seng, Y. K., Reason, C. J. C., . . . Yasunari, T. (2008). On the roles of the northeast cold surge, the Borneo vortex, the Madden-Julian Oscillation, and the Indian Ocean Dipole during the extreme 2006/2007 flood in southern Peninsular Malaysia. *Geophysical Research Letters, 35*(14). doi:https://doi.org/10.1029/2008GL033429

Thomas, B. F., Famiglietti, J. S., Landerer, F. W., Wiese, D. N., Molotch, N. P., & Argus, D. F. (2017). GRACE Groundwater Drought Index: Evaluation of California Central Valley groundwater drought. *Remote Sensing of Environment, 198*, 384-392. doi:https://doi.org/10.1016/j.rse.2017.06.026

Tirivarombo, S., Osupile, D., & Eliasson, P. (2018). Drought monitoring and analysis: Standardised Precipitation Evapotranspiration Index (SPEI) and Standardised Precipitation Index (SPI). *Physics and Chemistry of the Earth, Parts A/B/C, 106*, 1-10. doi:https://doi.org/10.1016/j.pce.2018.07.001

Torrence, C., & Webster, P. J. (1999). Interdecadal changes in the ENSO–monsoon system. *Journal of Climate, 12*(8), 2679-2690.

UNWATER. (2014). *Capacity Development to support National Drought Management Policy*. Retrieved from https://www.droughtmanagement.info/literature/UNW-DPC_NDMP_Country_Report_Malaysia_2014.pdf

Valipour, M. (2016). Optimization of neural networks for precipitation analysis in a humid region to detect drought and wet year alarms. *Meteorological Applications, 23*(1), 91-100. doi:10.1002/met.1533

Vicente-Serrano, S. M., Beguería, S., & López-Moreno, J. I. (2010). A Multiscalar Drought Index Sensitive to Global Warming: The Standardized Precipitation Evapotranspiration Index. *Journal of Climate, 23*(7), 1696-1718. doi:10.1175/2009jcli2909.1

Wang, A., Lettenmaier, D. P., & Sheffield, J. (2011). Soil Moisture Drought in China, 1950–2006. *Journal of Climate, 24*(13), 3257-3271. doi:10.1175/2011JCLI3733.1

Washington, R., & Preston, A. (2006). Extreme wet years over southern Africa: Role of Indian Ocean sea surface temperatures. *Journal of Geophysical Research: Atmospheres, 111*(D15). doi:10.1029/2005JD006724

Wells, N., Goddard, S., & Hayes, M. J. (2004). A Self-Calibrating Palmer Drought Severity Index. *Journal of Climate, 17*(12), 2335-2351. doi:10.1175/1520-0442(2004)017<2335:aspdsi>2.0.co;2

Wu, J., Miao, C., Tang, X., Duan, Q., & He, X. (2018). A nonparametric standardized runoff index for characterizing hydrological drought on the Loess Plateau, China. *Global and Planetary Change, 161*, 53-65. doi:https://doi.org/10.1016/j.gloplacha.2017.12.006

Xu, J., Ren, L. L., Ruan, X. H., Liu, X. F., & Yuan, F. (2012). Development of a physically based PDSI and its application for assessing the vegetation response to drought in northern China. *Journal of Geophysical Research: Atmospheres, 117*(D8).

Yang, Y., Dou, Y., Liu, D., & An, S. (2017). Spatial pattern and heterogeneity of soil moisture along a transect in a small catchment on the Loess Plateau. *Journal of Hydrology, 550*, 466-477. doi:https://doi.org/10.1016/j.jhydrol.2017.05.026

Yoon, J.-H., Mo, K., & Wood, E. F. (2012). Dynamic-Model-Based Seasonal Prediction of Meteorological Drought over the Contiguous United States. *Journal of Hydrometeorology, 13*(2), 463-482. doi:10.1175/JHM-D-11-038.1

Yusof, F., Hui-Mean, F., Suhaila, J., & Yusof, Z. (2013). Characterisation of Drought Properties with Bivariate Copula Analysis. *Water Resources Management, 27*(12), 4183-4207. doi:10.1007/s11269-013-0402-4

Zhai, J., Su, B., Krysanova, V., Vetter, T., Gao, C., & Jiang, T. (2010). Spatial Variation and Trends in PDSI and SPI Indices and Their Relation to Streamflow in 10 Large Regions of China. *Journal of Climate, 23*(3), 649-663. doi:10.1175/2009JCLI2968.1

Zhang, C. (2013). Madden–Julian oscillation: Bridging weather and climate. *Bulletin of the American Meteorological Society, 94*(12), 1849-1870.

Zhao, H., Gao, G., An, W., Zou, X., Li, H., & Hou, M. (2017). Timescale differences between SC-PDSI and SPEI for drought monitoring in China. *Physics and Chemistry of the Earth, Parts A/B/C, 102*, 48-58. doi:https://doi.org/10.1016/j.pce.2015.10.022

Tables

Table 1. Different drought levels based on the drought indices (Sun et al., 2018).

Table 2. The correlations between SPI/SPEI and PDSI from 3- to 24-month time scales. * indicates the correlation is statistically significant at p-value < 0.05.

Figures

Figure 1. Elevation (m a.s.l; green to brown colour shades) over Peninsular Malaysia. The whole Peninsular Malaysia is divided into four regions: East, South, North, and Central.

Figure 2. The diagram for data processing and analysis. The red boxes are related to data, orange boxes are calculated indices, and bule boxes are statistical analysis.

Figure 3. The trend pattern (per year) over Peninsular Malaysia based on SPI (a-d), SPEI (e-h) at 3-month, 6-month, 12-month and 24-month time scale, and PDSI (i). The black dots indicate significant values at 0.1 significance level according to the modified MK-test. Red to blue colour shades indicate different level of dryness and wetness, respectively.

Figure 4. The averaged PDSI against SPI and SPEI at 3-month, 6-month, 12-month, and 24-month time scales.

Figure 5. The percentage of area impacted by drought over Peninsular Malaysia. Drought are here estimated using SPI-6 (a), SPEI-6 (b), and PDSI (c), and at different levels of drought severity from no drought (D0, blue) to extreme drought (D5, dark red; cf. Table 1).

Figure 6. The precipitation deficits in 1983 (a), 1987 (b), 1993 (c) and 2005 (d) as compared to mean precipitation 1981-2019.

Figure 7. The REOF1 (a-d), REOF2 (e-h), and REOF3 (i-l) of SPI at 1-month, 6-month, 12-month, and 24-month time scale. The percentage indicates the fraction of variance of REOFs. Red to blue colour shades indicate different level of dryness and wetness, respectively.

Figure 8. The maps of regression coefficients of ENSO (a-d), SWIO (e-h) and QBO (i-l) for SPI at 3-month, 6-month, 12-month, and 24-month time scale. The black dots indicate statistically significant values at 0.1 significance level according to the asymptotically normal tests. Red to blue colour shades indicate negative and positive impacts of climate indices on SPI, respectively.

Figure 9. The maps of regression coefficients of ENSO (a-d), SWIO (e-h), and QBO (i-l) for SPEI at 3-month, 6-month, 12-month and 24-month time scale. The black dots indicate statistically significant values at 0.1 significance level according to the asymptotically normal tests. Red to blue colour shades indicate negative and positive impacts of climate indices on SPEI, respectively.

Figure 10. The maps of regression coefficients of ENSO, SWIO and QBO for PDSI. The black dots indicate statistically significant values at 0.1 significance level according to the asymptotically normal tests. Red to blue colour shades indicate negative and positive impacts of climate indices on PDSI, respectively.

Figure 11. The WTC analysis of the SPI-6 PCs and the ENSO, SWIO and QBO at different time scales. The thick black contour represents the 5% significance level against the red noise. The thin black line is the boundary of the cone of influence (COI), i.e., the edge effects caused by zero-padding effect. The phase lag is denoted by the arrow directions (right (left) is 0 (180) degree phase lag; up (down) is 270 (90) degree phase lag).

Figure 12. The surface climatological moisture flux with precipitation distribution (a), and moisture flux (divergence) regressed by ENSO, SWIO, and QBO during JJA (b-d). The (e-h) are similar as the (a-d) but for DJF. For (a) and (e), the magenta arrows and shaded area are climatological moisture flux and precipitation. For other figures, the arrows and shaded areas represent the regressed wind and regressed coefficients of moisture flux divergence. The magenta and black arrows in (b-d) and (f-h) are significant and non-significant results at p-value < 0.1, respectively. For shaded area, only significant results with the significance level of p-value < 0.1 are provided.

Tables

Table 1. Different drought levels based on the drought indices (Sun et al., 2018).

Drought level	SPI/SPEI	PDSI	Description
D0	DI > -0.5	DI > -1.0	No drought
D1	-1.0 < DI ≤ -0.5	-2.0 < DI ≤ -1.0	Mild drought
D2	-1.5 < DI ≤ -1.0	-3.0 < DI ≤ -2.0	Moderate drought
D3	-2.0 < DI ≤ -1.5	-4.0 < DI ≤ -3.0	Severe drought
D4	DI ≤ -2.0	DI ≤ -4.0	Extreme drought

Table 2. The correlations between SPI/SPEI and PDSI from 3- to 24-month time scales. * indicates the correlation is statistically significant at p-value < 0.05.

	3-month	6-month	12-month	24-month
SPI	0.599*	0.617*	0.577*	0.452*
SPEI	0.613*	0.622*	0.586*	0.466*

Figures

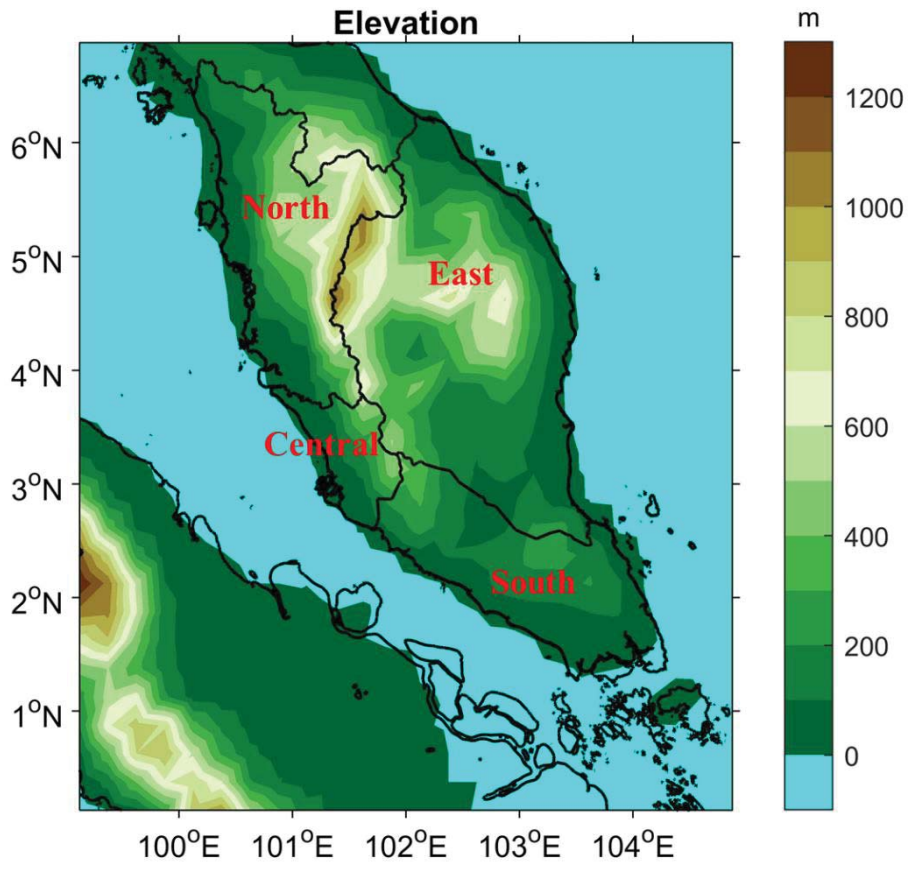

Figure 1. Elevation (m a.s.l; green to brown colour shades) over Peninsular Malaysia. The whole Peninsular Malaysia is divided into four regions: East, South, North, and Central.

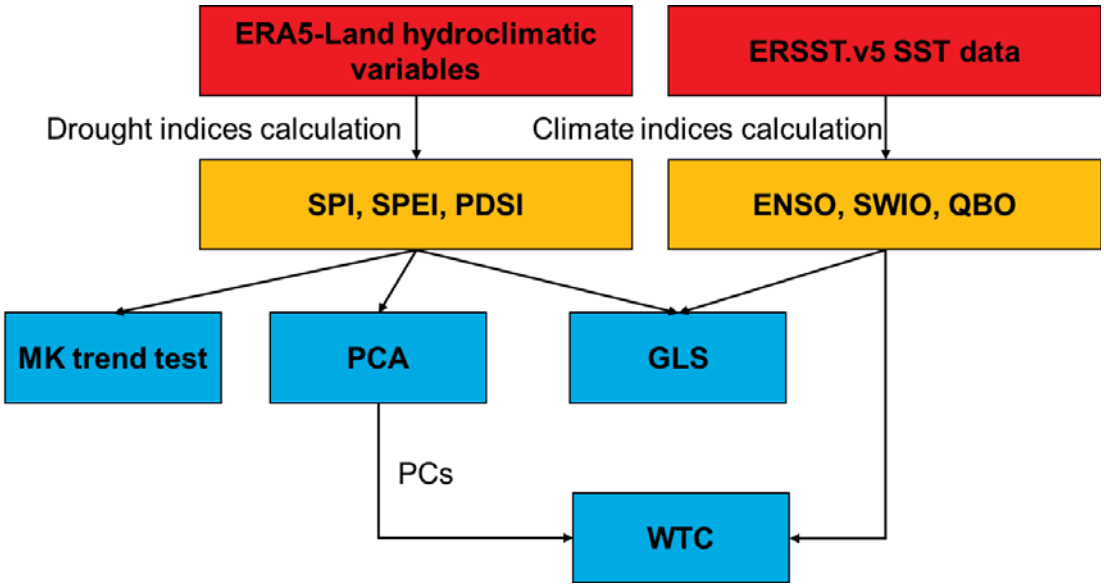

Figure 2. The diagram for data processing and analysis. The red boxes are related to data, orange boxes are calculated indices, and bule boxes are statistical analysis.

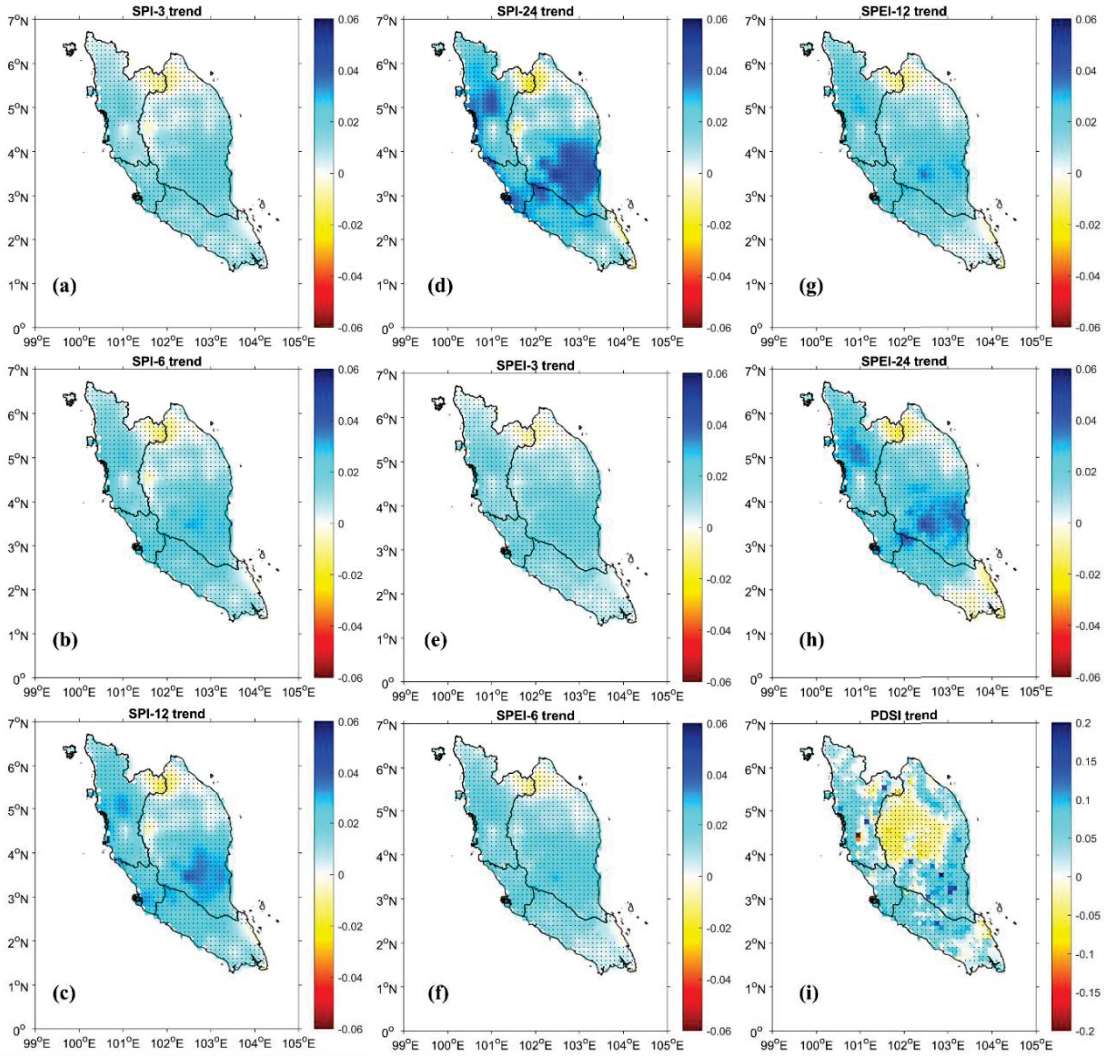

Figure 3. The trend pattern (per year) over Peninsular Malaysia based on SPI (a-d), SPEI (e-h) at 3-month, 6-month, 12-month and 24-month time scale, and PDSI (i). The black dots indicate significant values at 0.1 significance level according to the modified MK-test. Red to blue colour shades indicate different level of dryness and wetness, respectively.

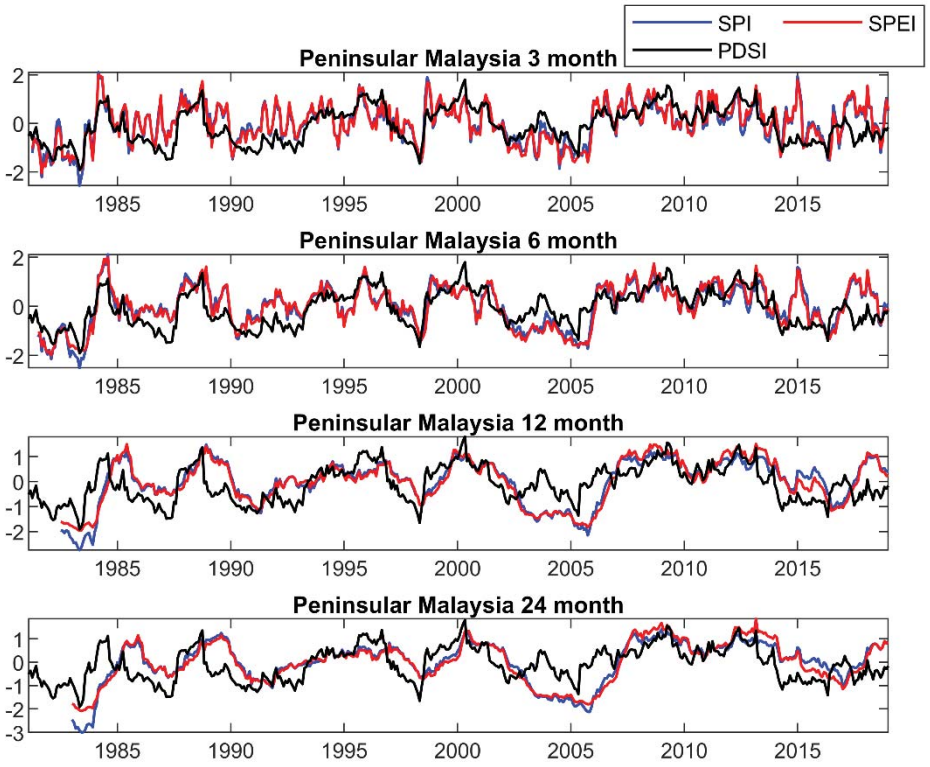

Figure 4. The averaged PDSI against SPI and SPEI at 3-month, 6-month, 12-month, and 24-month time scales.

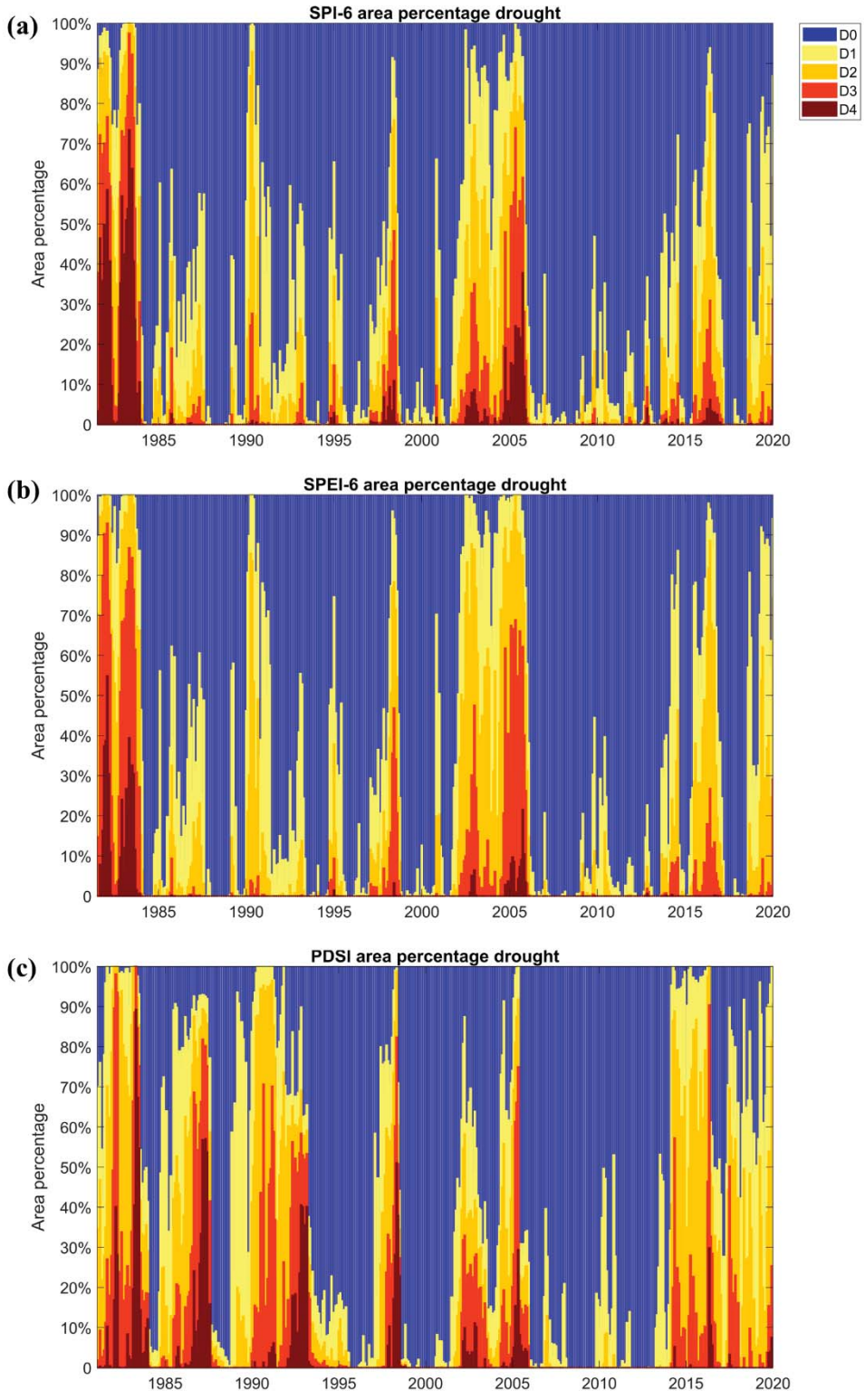

Figure 5. The percentage of area impacted by drought over Peninsular Malaysia. Drought are here estimated using SPI-6 (a), SPEI-6 (b), and PDSI (c), and at different levels of drought severity from no drought (D0, blue) to extreme drought (D5, dark red; cf. Table 1).

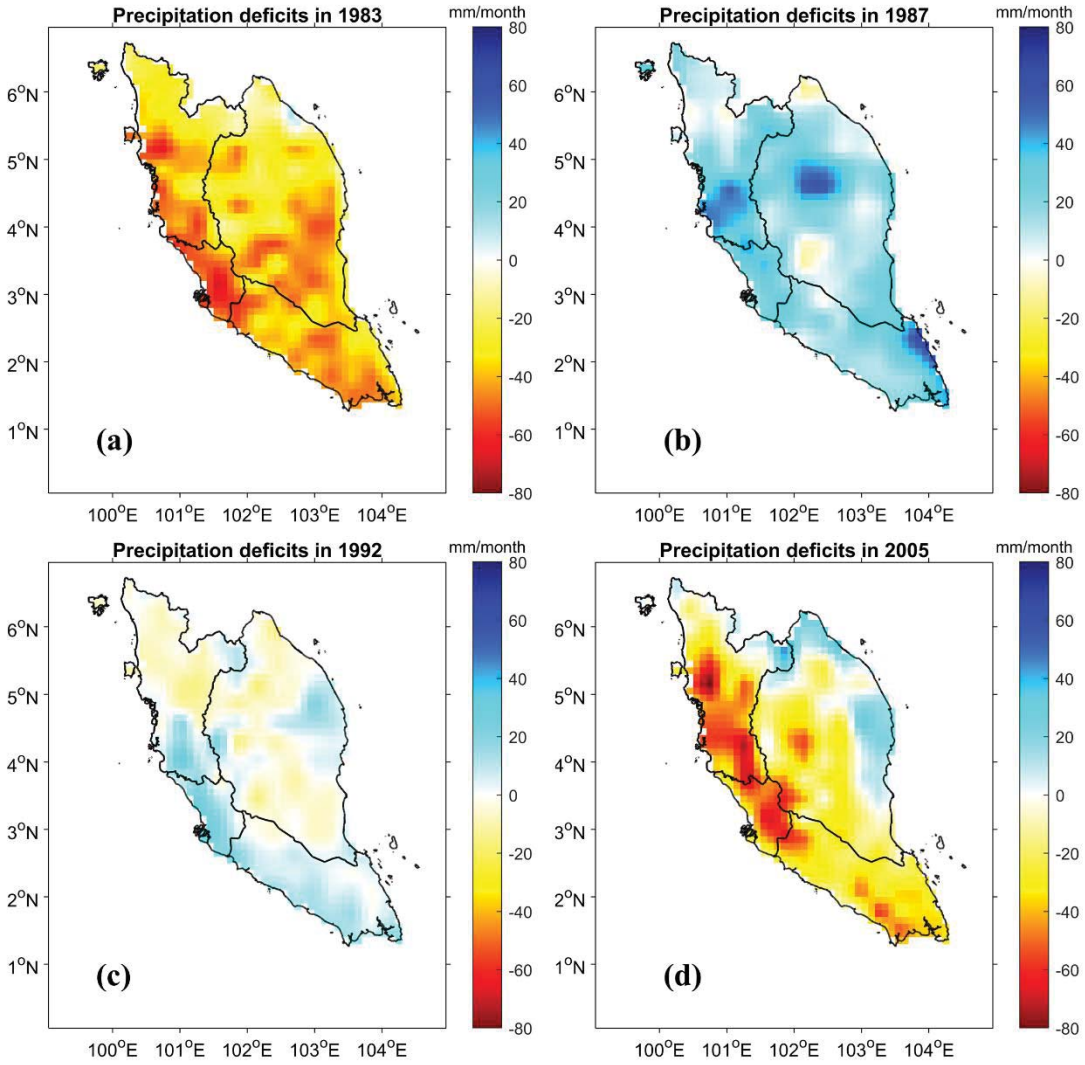

Figure 6. The precipitation deficits in 1983 (a), 1987 (b), 1993 (c) and 2005 (d) as compared to mean precipitation 1981-2019.

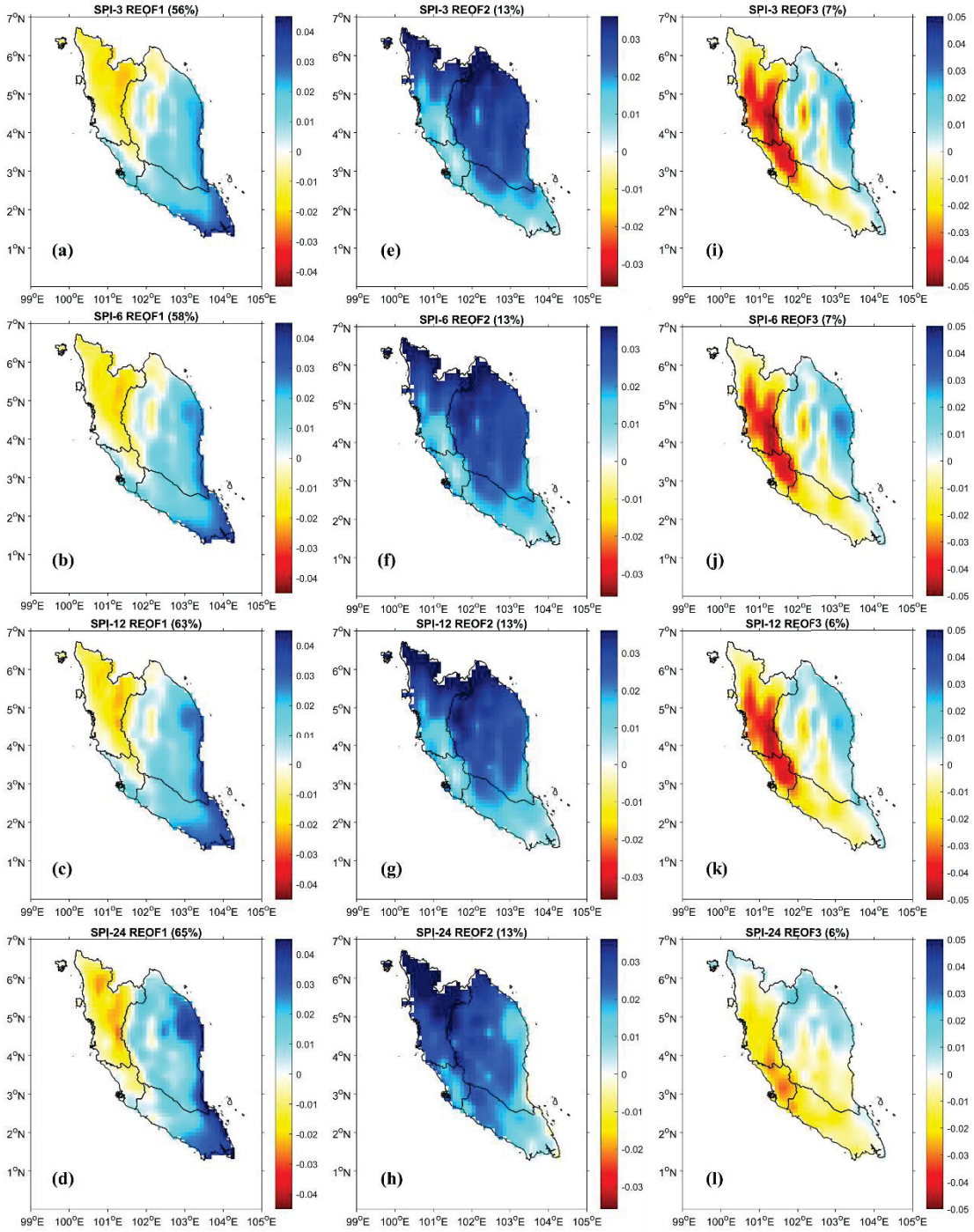

Figure 7. The REOF1 (a-d), REOF2 (e-h), and REOF3 (i-l) of SPI at 1-month, 6-month, 12-month, and 24-month time scale. The percentage indicates the fraction of variance of REOFs. Red to blue colour shades indicate different level of dryness and wetness, respectively.

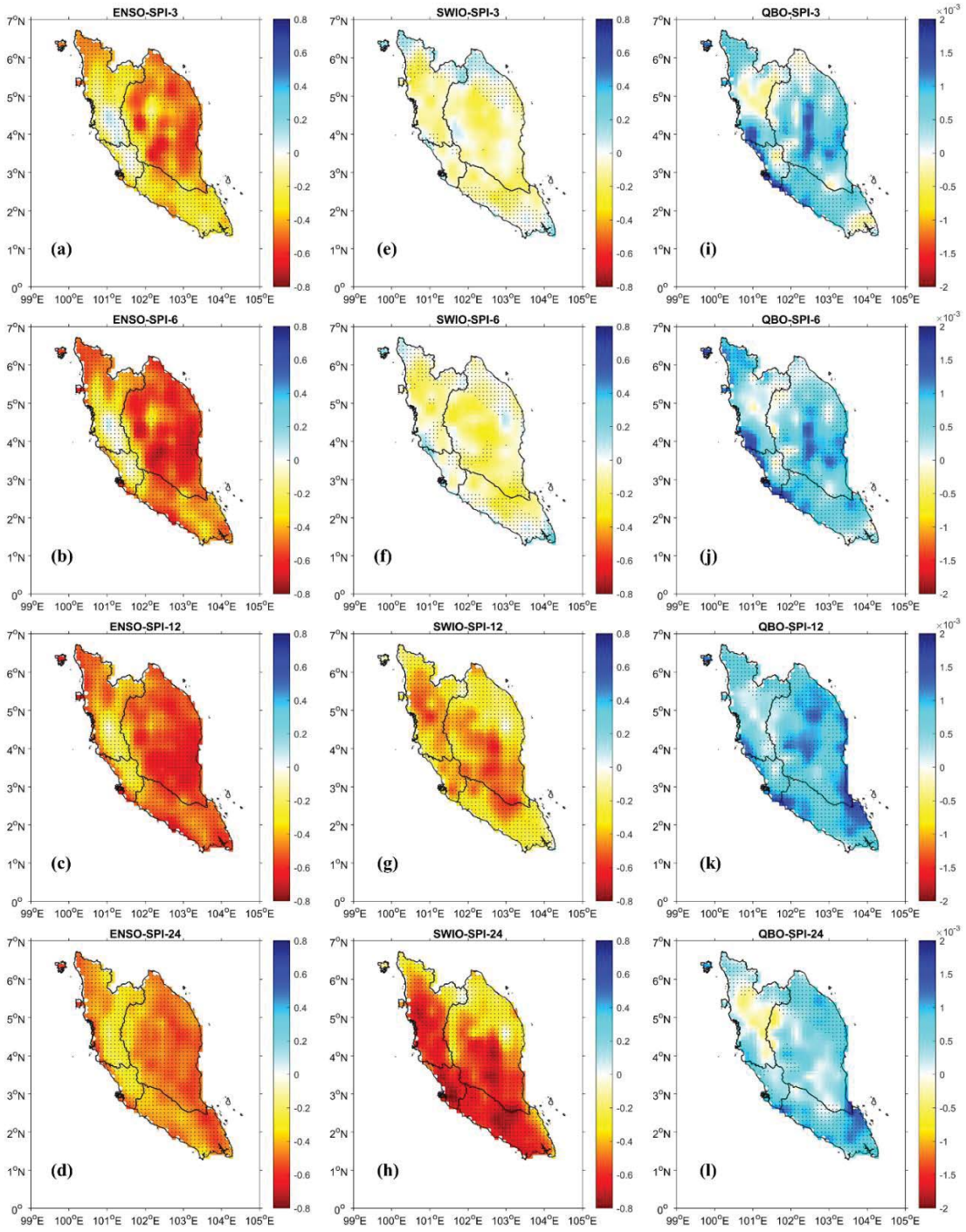

Figure 8. The maps of regression coefficients of ENSO (a-d), SWIO (e-h) and QBO (i-l) for SPI at 3-month, 6-month, 12-month, and 24-month time scale. The black dots indicate statistically significant values at 0.1 significance level according to the asymptotically normal tests. Red to blue colour shades indicate negative and positive impacts of climate indices on SPI, respectively.

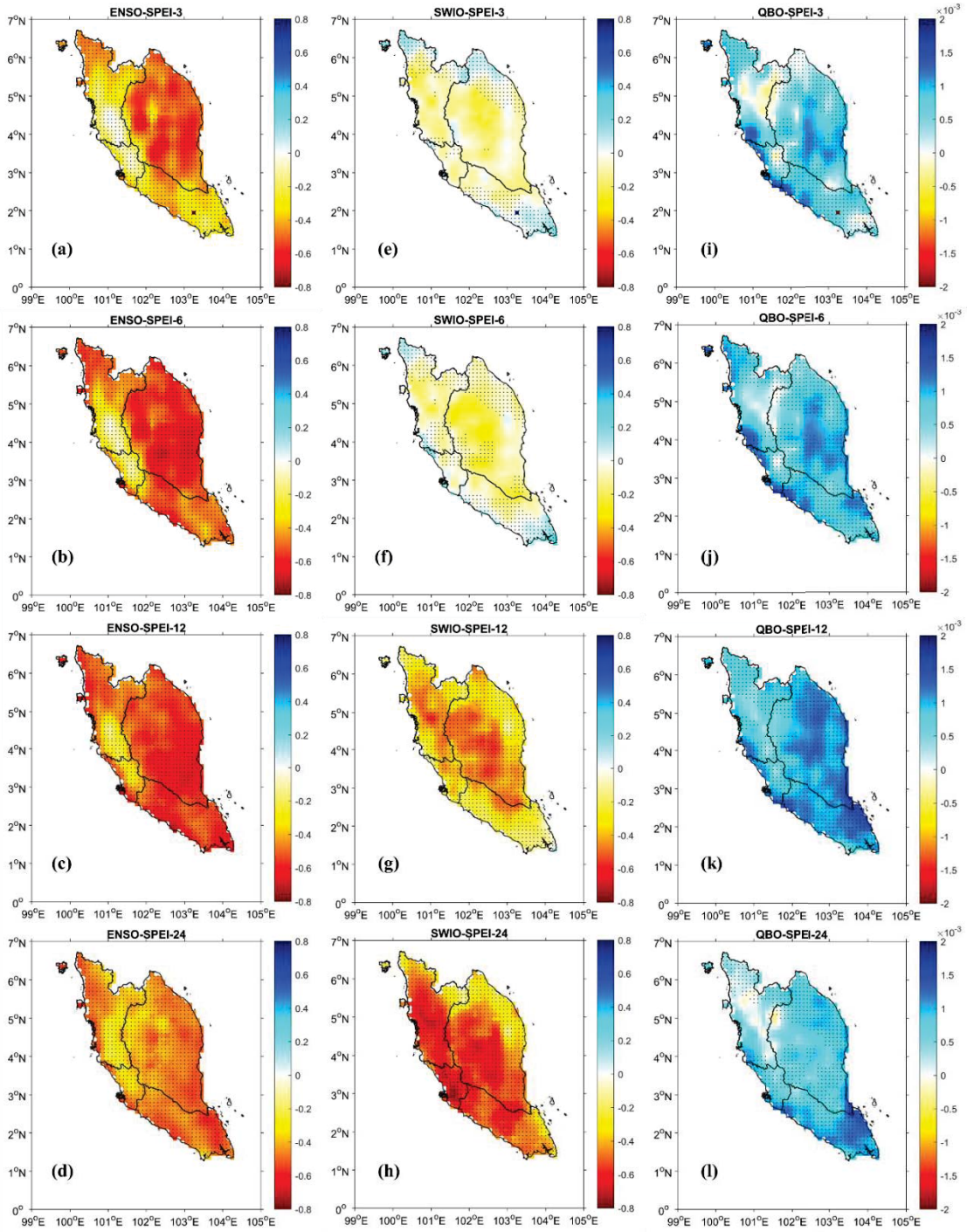

Figure 9. The maps of regression coefficients of ENSO (a-d), SWIO (e-h), and QBO (i-l) for SPEI at 3-month, 6-month, 12-month and 24-month time scale. The black dots indicate statistically significant values at 0.1 significance level according to the asymptotically normal tests. Red to blue colour shades indicate negative and positive impacts of climate indices on SPEI, respectively.

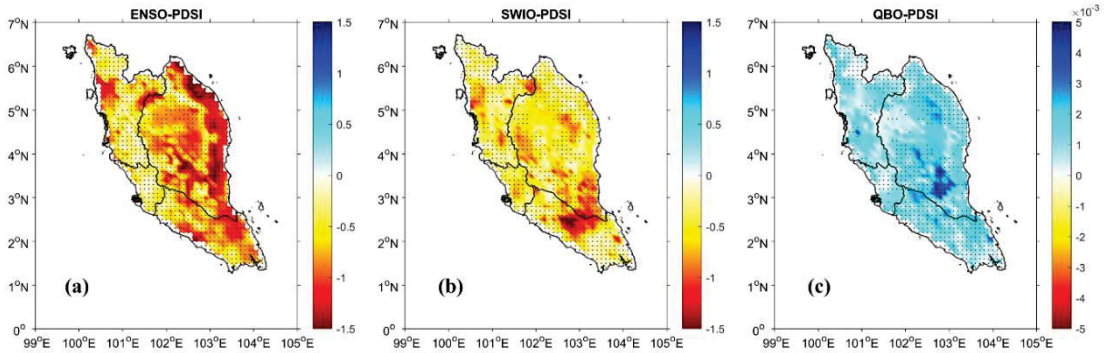

Figure 10. The maps of regression coefficients of ENSO, SWIO and QBO for PDSI. The black dots indicate statistically significant values at 0.1 significance level according to the asymptotically normal tests. Red to blue colour shades indicate negative and positive impacts of climate indices on PDSI, respectively.

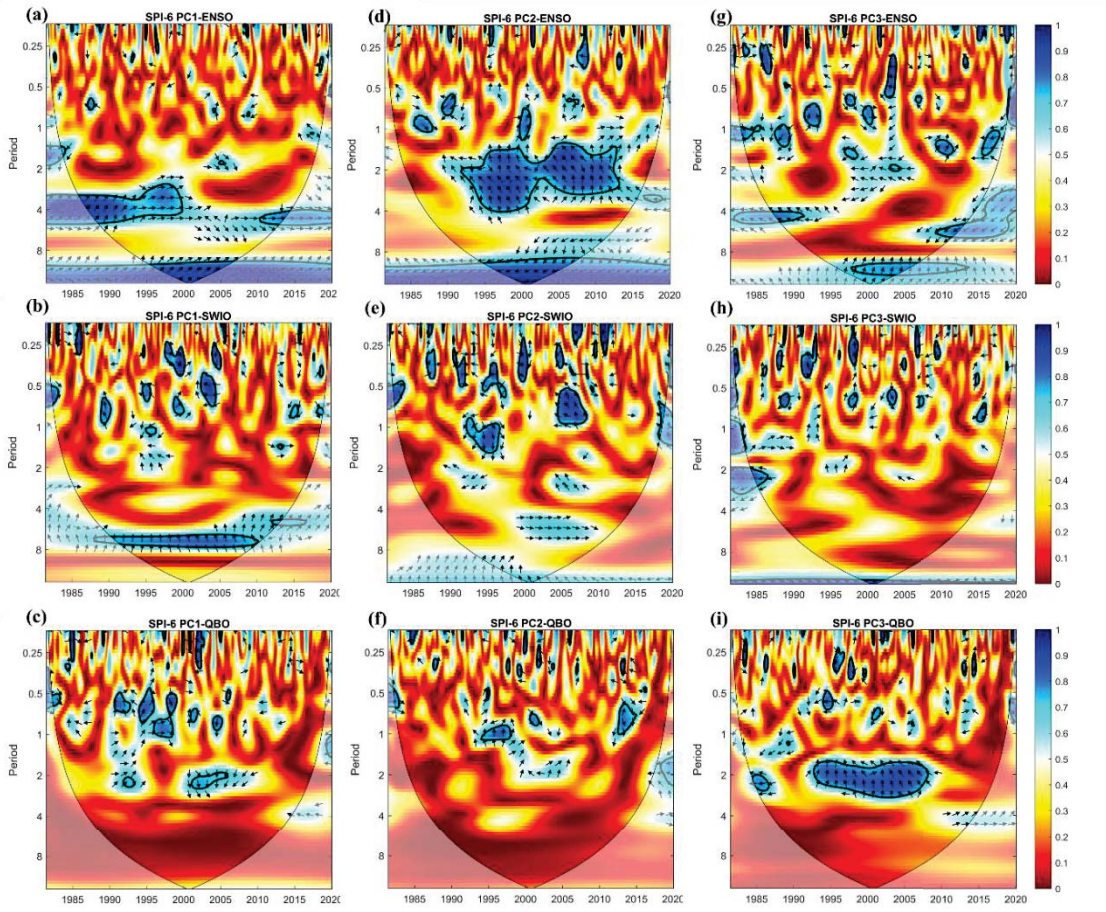

Figure 11. The WTC analysis of the SPI-6 PCs and the ENSO, SWIO and QBO at different time scales. The thick black contour represents the 5% significance level against the red noise.

The thin black line is the boundary of the cone of influence (COI), i.e., the edge effects caused by zero-padding effect. The phase lag is denoted by the arrow directions (right (left) is 0 (180) degree phase lag; up (down) is 270 (90) degree phase lag).

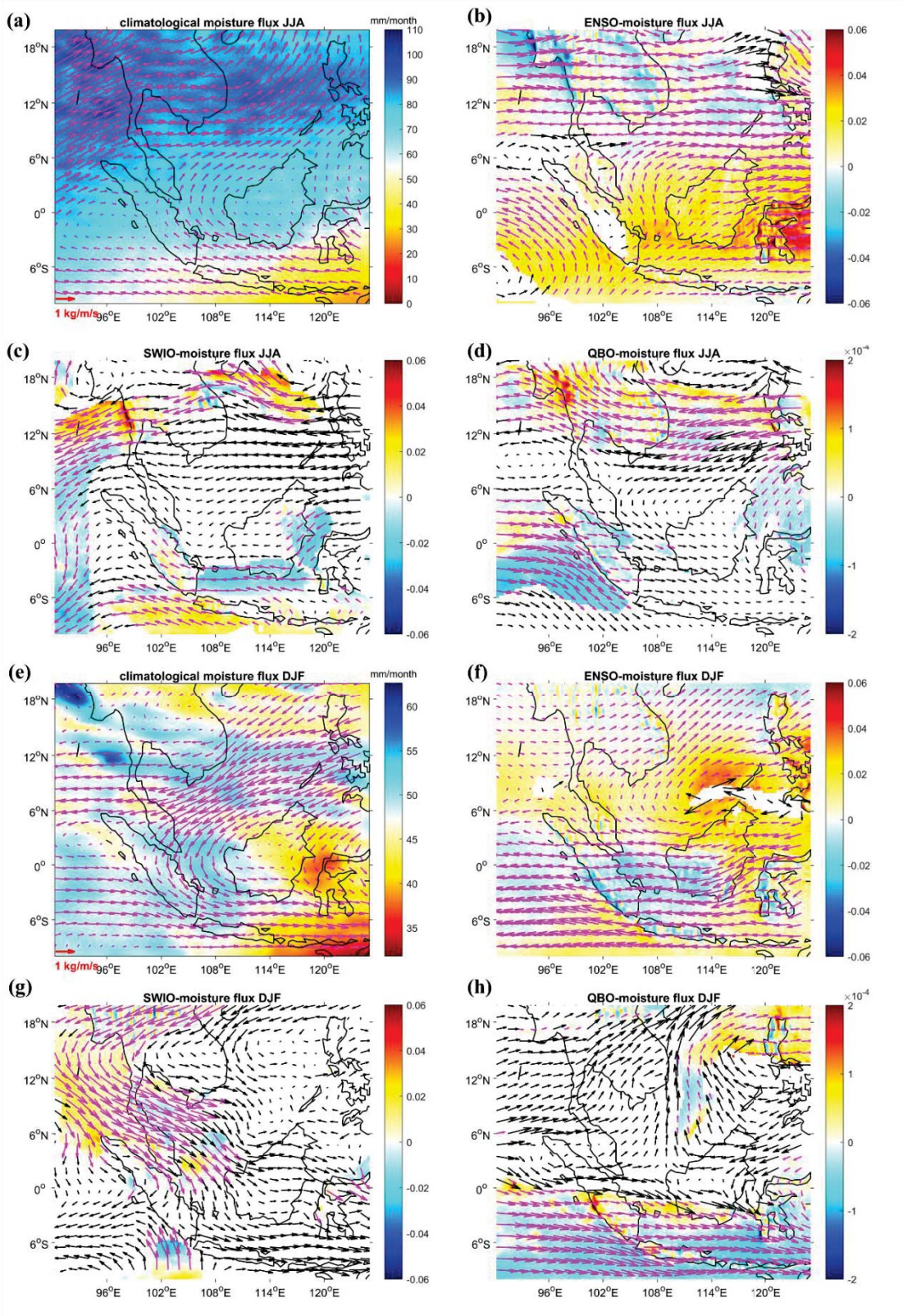

Figure 12. The surface climatological moisture flux with precipitation distribution (a), and moisture flux (divergence) regressed by ENSO, SWIO, and QBO during JJA (b-d). The (e-h) are similar as the (a-d) but for DJF. For (a) and (e), the magenta arrows and shaded area are climatological moisture flux and precipitation. For other figures, the arrows and shaded areas represent the regressed wind and regressed coefficients of moisture flux divergence. The magenta and black arrows in (b-d) and (f-h) are significant and non-significant results at p-value < 0.1, respectively. For shaded area, only significant results with the significance level of p-value < 0.1 are provided.

Appendix

PDSI calculation

The calculation of the PDSI is performed as follows (Liu et al., 2013; Wells et al., 2004):

$$PDSI_i = p \times PDSI_{i-1} + q \times Z_i \quad \text{(A1)}$$

where $PDSI_i$ and $PDSI_{i-1}$ are the current and previous month's PDSI, respectively. p and q are the empirical duration factors, which are adjusted using the self-calibrating procedure. Z_i is the current moisture anomaly index, and can be expressed as:

$$Z_i = K_i \times D_i \quad \text{(A2)}$$

where D_i is the moisture departure, written as

$$D_i = P - \left(\frac{\overline{ET_i}}{\overline{PE_i}}PE + \frac{\overline{R_i}}{\overline{PR_i}}PR + \frac{\overline{RO_i}}{\overline{PRO_i}}PRO - \frac{\overline{L_i}}{\overline{PL_i}}PL\right) \quad \text{(A3)}$$

where P is the precipitation. ET, R, RO and L are the evapotranspiration, recharge, runoff and loss of soil moisture, respectively. PE, PR, PRO and PL are the potential evapotranspiration, recharge, runoff and loss of soil moisture, respectively.

K_i is the current climate characteristics value and a refinement of K_i' (i.e., the Palmer's general approximation of climate characteristics). It is written as:

$$K_i = \left(\frac{17.67}{\sum_{j=1}^{12} \overline{D_j} \times K_j'}\right) K_i' \quad \text{(A4)}$$

$$K_i' = 1.5 \times log\left[\left(\frac{\overline{PE_i} + \overline{R_i} + \overline{RO_i}}{\overline{P_i} + \overline{L_i}} + 2.8\right) / \overline{D_i}\right] + 0.5 \quad \text{(A5)}$$

Figure A1. The scatterplot and correlations between ERA5 and observed precipitation.

Figure A2. The relative importance analysis for the Indian variability indices to the SPI over Peninsular Malaysia.

Figure A3. The SST anomaly shows the warm and cold phase of the ENSO during 1900 and 2019.

Figure A4. The SPI PCs and SPI at 3-, 6-, 12-, and 24-month time scale.

Figure A5. The scatterplot between REOF2 and REOF3 of SPI-3.

Figure A6. The REOF1 (a-d), REOF2 (e-h), and REOF3 (i-l) of SPEI at 1-month, 6-month, 12-month and 24-month time scale.

Figure A7. The REOF1 (a), REOF2 (b), and REOF3 (c) of PDSI.

Appendix Figures

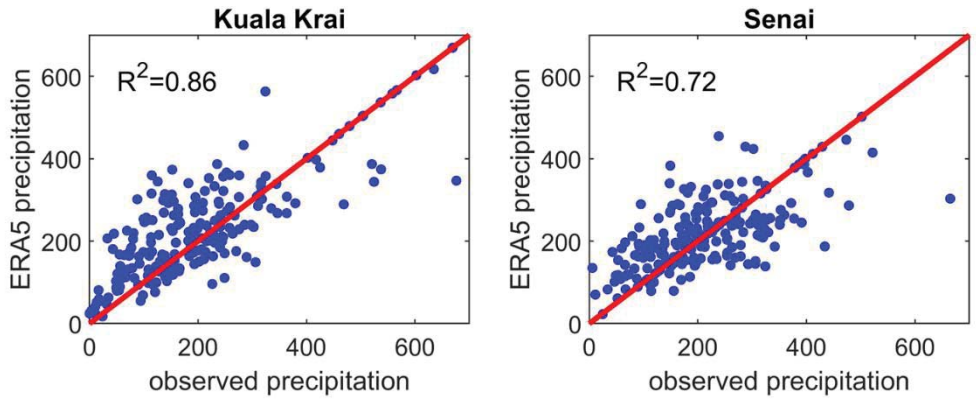

Figure A1. The scatterplot and correlations between ERA5 and observed precipitation.

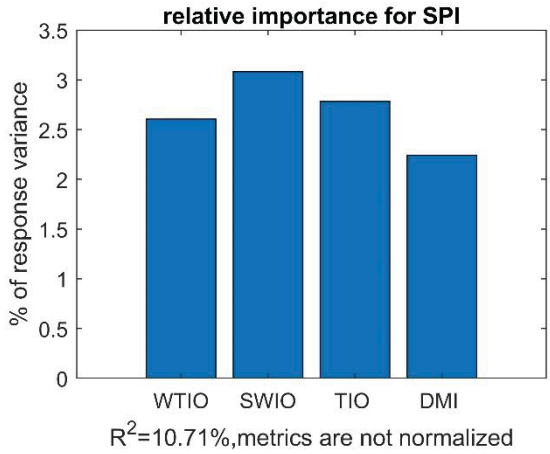

Figure A2. The relative importance analysis for the Indian variability indices to the SPI over Peninsular Malaysia.

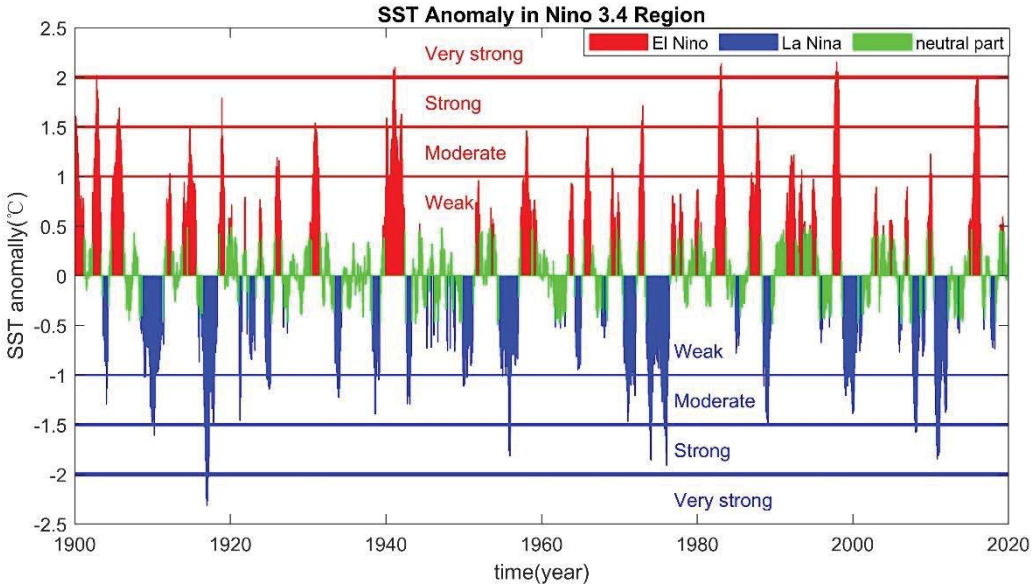

Figure A3. The SST anomaly shows the warm and cold phase of the ENSO during 1900 and 2019.

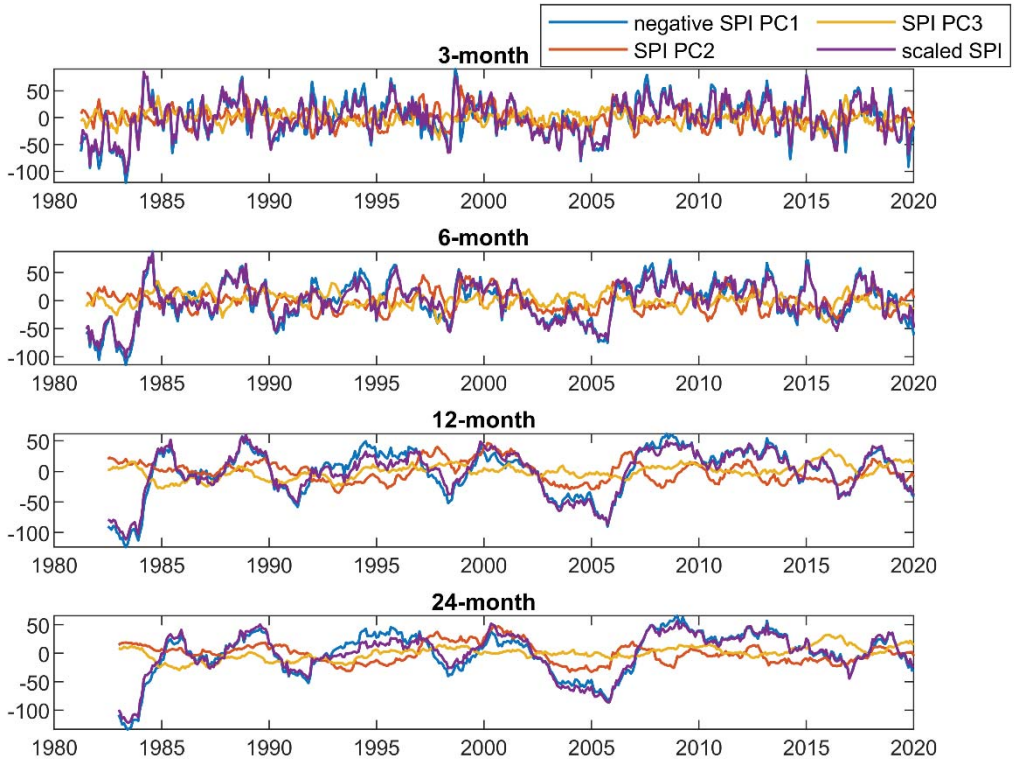

Figure A4. The SPI PCs and SPI at 3-, 6-, 12-, and 24-month time scale.

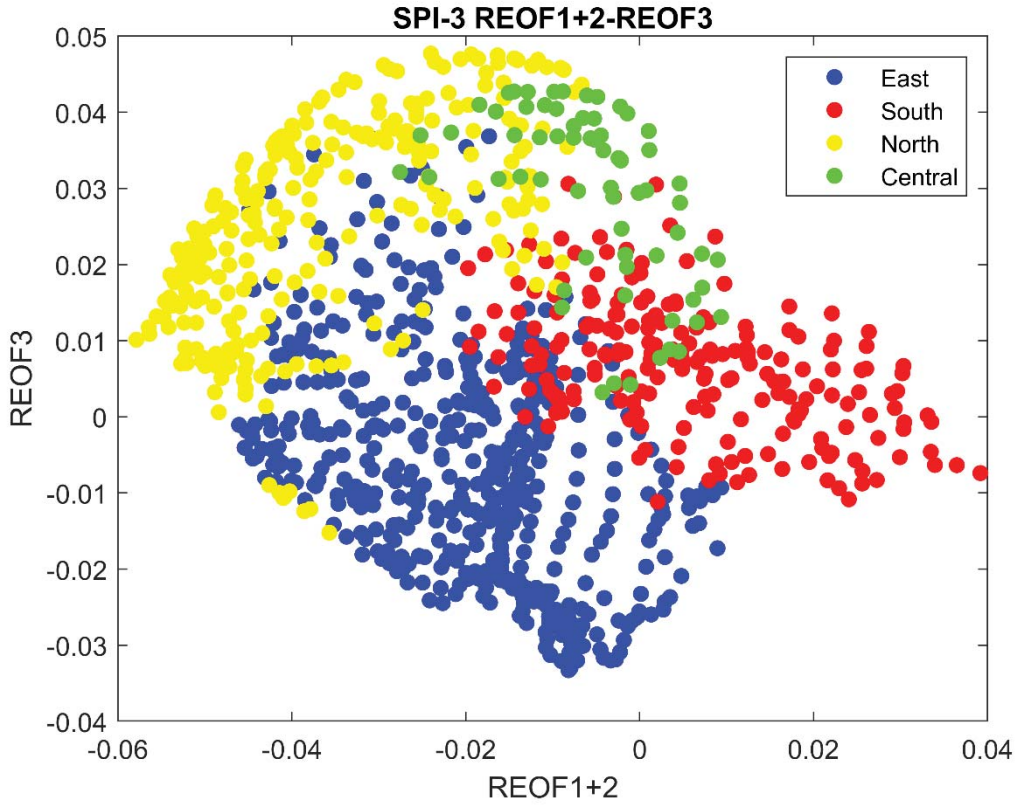

Figure A5. The scatterplot between REOF1+REOF2 and REOF3 of SPI-3.

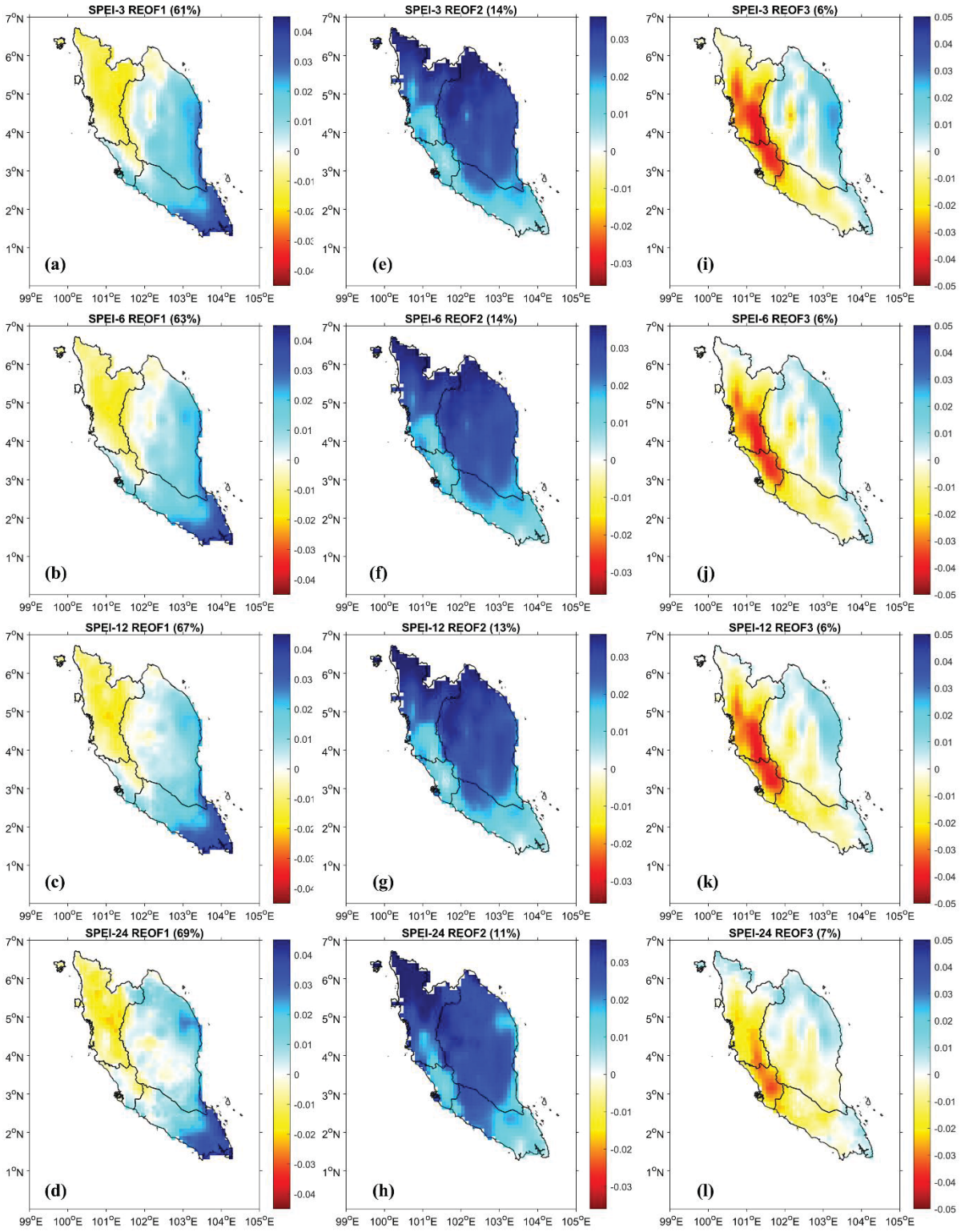

Figure A6. The REOF1 (a-d), REOF2 (e-h), and REOF3 (i-l) of SPEI at 1-month, 6-month, 12-month and 24-month time scale.

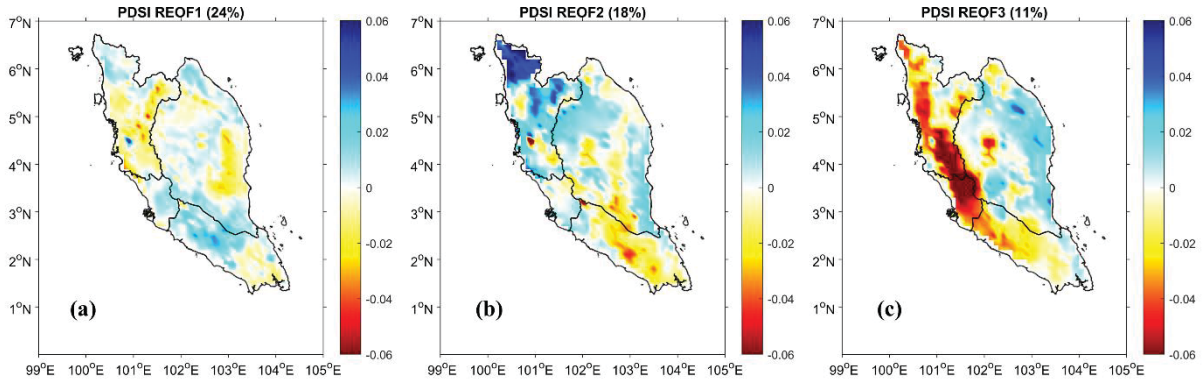

Figure A7. The REOF1 (a), REOF2 (b), and REOF3 (c) of PDSI.